



This is to certify that the

thesis entitled
CHEMICAL VARIATION OF THE TEPHRA FALL BENEATH THE
RAINIER MESA ASH FLOW SHEET: IMPLICATIONS FOR
INCREMENTAL GROWTH OF A LARGE MAGMA BODY

presented by

Kristin Terese Huysken

has been accepted towards fulfillment of the requirements for

M.S. degree in <u>Geologica</u>l Sciences

Major professor

Date _____

O-7639

MSU is an Affirmative Action/Equal Opportunity Institution

LIBRARY Michigan State University

PLACE IN RETURN BOX to remove this checkout from your record.

TO AVOID FINES return on or before date due.

DATE DUE	DATE DUE	DATE DUE
	·	

MSU Is An Affirmative Action/Equal Opportunity Institution c;circidatedus.pm3-p.1

CHEMICAL VARIATION OF THE TEPHRA FALL BENEATH THE RAINIER MESA ASH-FLOW SHEET: IMPLICATIONS FOR INCREMENTAL GROWTH OF A LARGE MAGMA BODY

Ву

Kristin Terese Huysken

A THESIS

Submitted to
Michigan State University
in partial fulfillment of the requirements
for the degree of

MASTER OF SCIENCE

Department of Geological Sciences

1993

ABSTRACT

CHEMICAL VARIATION OF THE TEPHRA-FALL BENEATH THE RAINIER MESA ASH-FLOW SHEET: IMPLICATIONS FOR INCREMENTAL GROWTH OF A LARGE MAGMA BODY

By

Kristin Terese Huysken

Tephra-fall deposits underlying, and associated with, largevolume, chemically zoned ash-flow sheets have been thought to represent the uppermost fractionated portion of large zoned magma bodies. This hypothesis is evaluated by analyzing the tephra-fall deposits beneath the voluminous, chemically-zoned Rainier Mesa ashflow sheet. Significant chemical variation in both whole rock and individual pumice samples indicates that the eruptive processes may be more complex than this simple interpretation suggests. The tephra-fall deposits span the entire chemical range (approximately 67-78% SiO2) of the high-silica portion of the Rainier Mesa ash-flow sheet. Significant chemical zoning of small ash-flow layers within the tephra-fall sequence are consistent with eruption from a small chemically zoned magma body. Increased upsection chemical evolution among the small ash-flow layers indicates that the magma became increasingly evolved with time. Because of the very small volume of the small ash-flow layers, and the significant chemical variation within each layer (up to 6% variation in SiO₂), the large volume Rainier Mesa magma body could not have been in place before the eruption of the tephra-fall sequence. The Rainier Mesa magma body may have been incrementally emplaced and periodically erupting throughout its emplacement history. This has general implications for the emplacement and evolution of large-volume magma bodies.

ACKNOWLEDGMENTS

First, I thank my family, especially my parents Bud and Micki Huysken, for ever present emotional and financial support throughout the course of my education.

Sincere appreciation and thanks are extended to my advisor, Tom Vogel, for his thoughtful insight, intense interest, and willingness to offer guidance relating to both this thesis and to my education in general. I am grateful to my committee members Bill Cambray, Dave Matty, and Kaz Fujita. They have provided useful discussion throughout the course of this project, as well as helpful and appreciated comments in their review of this thesis. I am especially grateful to Dave Matty for sparking my interest in igneous processes and (along with Steve Stahl and Reed Wicander) steering in the direction of graduate school.

I thank Larry McKague and Lee Younker for their parts in getting me to the Test Site each year and Larry McKague for the excellent photographs of the tephra-fall sequence. I would like to acknowledge Bill McKinnis and Barbara for their assistance at the Test Site.

Thanks to Tim Flood for his very insightful discussions, and intense excitement regarding this project. Thanks also to

Jim Mills for the excellent dissertation on the Timber Mountain Tuff. The information was invaluable to the prosecution of this study.

Fellow petrology students Tom Weaver and Tim Woodburne are thanked for their camaraderie and moral support.

Finally, special thanks go to Matt Casselton, Alex Guimaraes, and Maureen Walton who couldn't be closer if they were family.

TABLE OF CONTENTS

LIST OF FIGURESvi
INTRODUCTION
Rainier Mesa Member2
Magma Evacuation Dynamics4
DESCRIPTION OF THE TEPHRA-FALL SEQUENCE
SAMPLE SELECTION AND PREPARATION13
MAJOR ELEMENT VARIATION18
TRACE ELEMENT VARIATION25
CHEMICAL VARIATION WITH STRATIGRAPHIC POSITION30
RARE EARTH ELEMENT VARIATION36
DISCUSSION39
APPENDICES49
BTBLTOGRAPHY80

LIST OF FIGURES

Figure	1.	Location of the Southwest Nevada Volcanic Field
Figure	2.	Zr vs. silica for the Rainier Mesa ash-flow sheet and the underlying tephra-fall sequence
Figure	3.	Schematic eruption dynamics of the Rainier Mesa ash-flow sheet6
Figure	4.	Generalized stratigraphy of major volcanic units of the Southwest Nevada Volcanic Field and approximate ages8
Figure	5.	Tephra-fall sequence underlying the Rainier Mesa ash-flow sheet10
Figure	6.	a.) Small ash-flow layer within the tephra-fall sequence. b.) 52 m ash flow within the tephra-fall sequence11
Figure	7.	Generalized stratigraphic column of the tephra-fall sequence at a.) Rainier Mesa location and b.) Pahute Mesa location14
Figure	8.	Major element variation of small ash-flow layers within the tephra-fall sequence and the overlying Rainier Mesa ash-flow sheet
Figure	9.	Trace element variation of small ash-flow layers within the tephra-fall sequence and the overlying Rainier Mesa ash-flow sheet
Figure	10.	Major and trace element variation with stratigraphic position (depth), for small ash-flow layers within the tephra-fall sequence31

LIST OF FIGURES (continued)

Figure	11.	Chondrite normalized REE patterns for small ash-flow layers within the tephra-fall sequence and the high-silica portion of the Rainier Mesa ash-flow sheet
Figure	12.	Average REE abundances for small ash-flow layers within the tephra-fall sequence
Figure	13.	Schematic diagram depicting the interpreted emplacement of the Rainier Mesa magma body44

INTRODUCTION

The Rainier Mesa ash-flow sheet contains an extremely large chemical variation. It is a large (1200 km³), 11.6 m.y. old cooling unit that ranges in composition from 56 to 78% SiO₂ (Mills, 1991). Ninety percent of the Rainier Mesa ash flow possesses a silica content greater than 66%, and is defined by Mills (1991) as the high-silica portion of the ash-flow sheet.

Large volume ash-flow sheets are of great importance in interpreting high-level magmatic systems. They represent a virtually instantaneous sampling of a large portion of the magma body (Smith, 1979; Hildreth, 1981). Accordingly, numerous studies indicate that the chemical stratigraphy of outflow sheets produced by these eruptions is inversely related to the chemical zoning within the magma body (e.g. Smith, 1979; Hildreth, 1981). In a general way, most chemically-zoned ash-flow sheets correspond to this simple picture.

Whereas many pyroclastic flows represent, in large scale, a stratigraphic inversion of chemical zoning in the magma body, many are also complicated by complex eruption dynamics, multiple vents, topographic barriers, and pyroclastic flow dynamics (Trial and Spera, 1990). Numerical calculations indicate that compositional breaks and complex cooling breaks can be caused solely by the dynamics of pyroclastic flow (Valentine, et al., 1991, 1992).

Regardless of these complexities, eruption of a chemically zoned system typically begins with the eruption of the highest silica upper portion of the magma followed by the lower, more mafic component as time progresses (Blake, 1981).

Small pre-caldera eruptive deposits are just as important in understanding the mechanics of large volume magmatic systems as the main ash-flow sheet. These deposits are usually thought to be pre-eruptive "burps" from the uppermost, high silica portion of the larger magma body. For this reason, they have often been neglected in studies of voluminous magmatic systems.

A tephra-fall sequence occurs immediately beneath the Rainier Mesa ash-flow sheet at two locations on the Nevada Test Site (NTS). Eruptions which produced these deposits were precursors to the large caldera-forming eruption.

Rainier Mesa Member

The Rainier Mesa Member is a 1200 km³ ash flow sheet, the eruption of which led to the collapse of the Timber Mountain Caldera approximately 11.6 m.y. ago (Byers et al., 1976; Broxton et al., 1989). It is part of a system of seven calderas that make up the Southwest Nevada Volcanic Field (SWNVF) (Fig. 1). This voluminous deposit is chemically and mineralogically zoned and has been interpreted by Mills (1991) to be the result of eruption from a chemically stratified chamber. Chemical variations within the Rainier Mesa Member

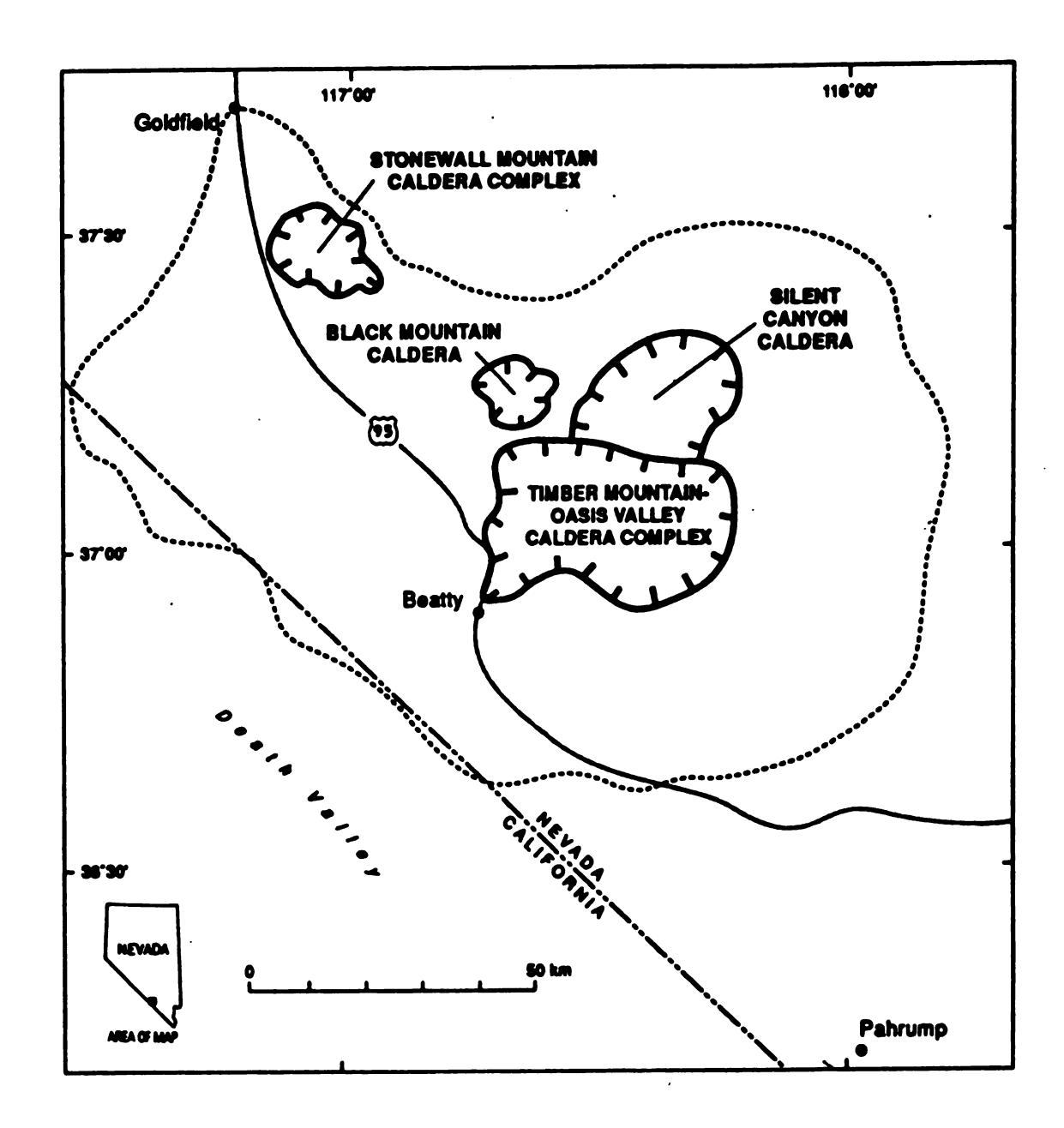


Figure 1. Location of the Southwest Nevada Volcanic Field. The dashed line outlines the extent of the Timber Mountain Tuff. The Timber Mountain Calderas, Oasis Valley Caldera, Claim Canyon Caldera Segment, and Sleeping Butte Caldera Segment are reported as the Timber Mountain-Oaisis Valley Caldera Complex (after Carr et al., 1984; Noble et al., 1984; and Vogel et al., 1987).

indicate both a high silica (approximately 66-78%) and low silica trends (approximately 56-66%) (Mills, 1991). Figure 2 illustrates these trends through SiO^2 -Zr relationships.

Beneath the Rainier Mesa Member lie a series of layered tephra-fall deposits interbedded with small, discrete ash-flow layers. The purpose of this study is to test whether the tephra-fall sequence underlying the Rainier Mesa ash-flow sheet represents eruption from the uppermost fractionated portion of the Rainier Mesa magma body.

Magma Evacuation Dynamics

A simple model of chamber evacuation (Fig. 3) illustrates magma withdrawal from a layered system occurring radially, where magma is drawn toward the eruptive vent from all directions (Blake, 1981; Blake and Ivey, 1986; Spera, 1983; Spera et al., 1986). Figure 3 is a schematic diagram illustrating the dynamics of chamber evacuation. Evacuation isochrons illustrate the position of the magma that will simultaneously reach the vent as eruption progresses. The high-silica and lower-silica fields indicate compositional layering in a chemically layered and zoned system, and the arrows show the direction of magma movement toward the vent. Over time, eruption taps progressively deeper levels of the chamber while still maintaining contribution from the roof magma. The resulting deposits are a collection of compositionally zoned tephra deposits consisting of a more

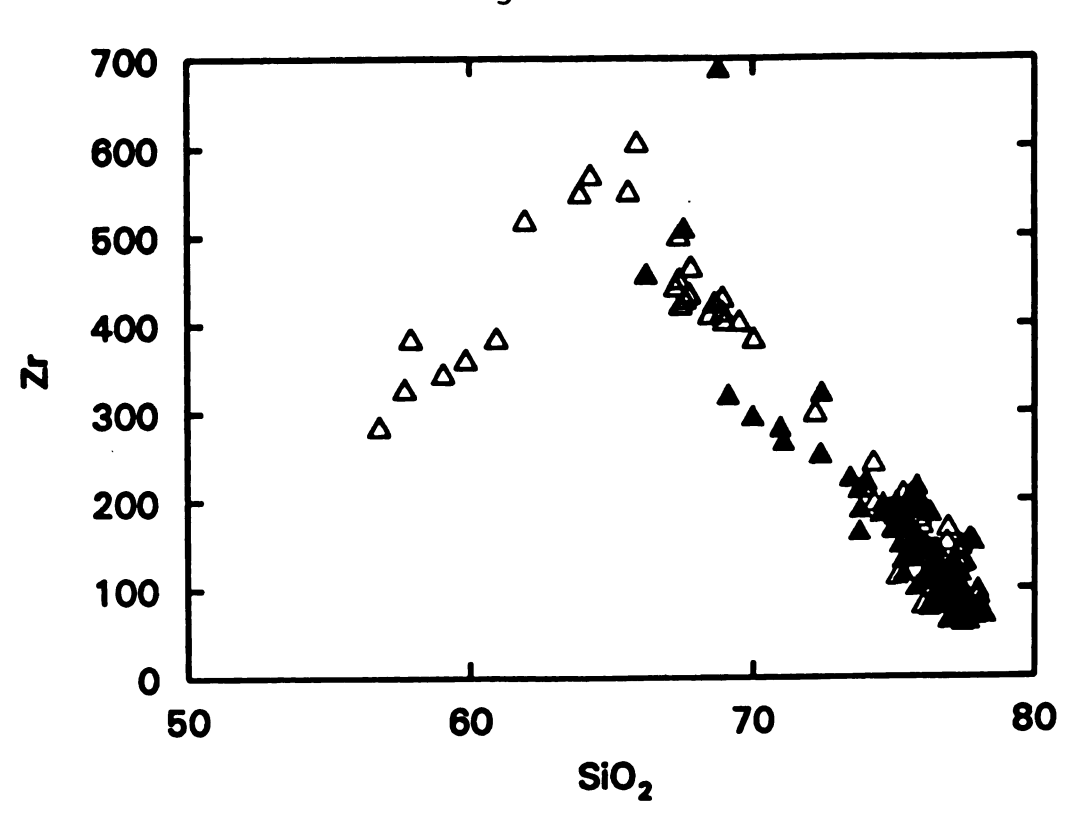


Figure 2. Zr vs. silica for the Rainier Mesa as-flow sheet and the underlying tephra-fall sequence.

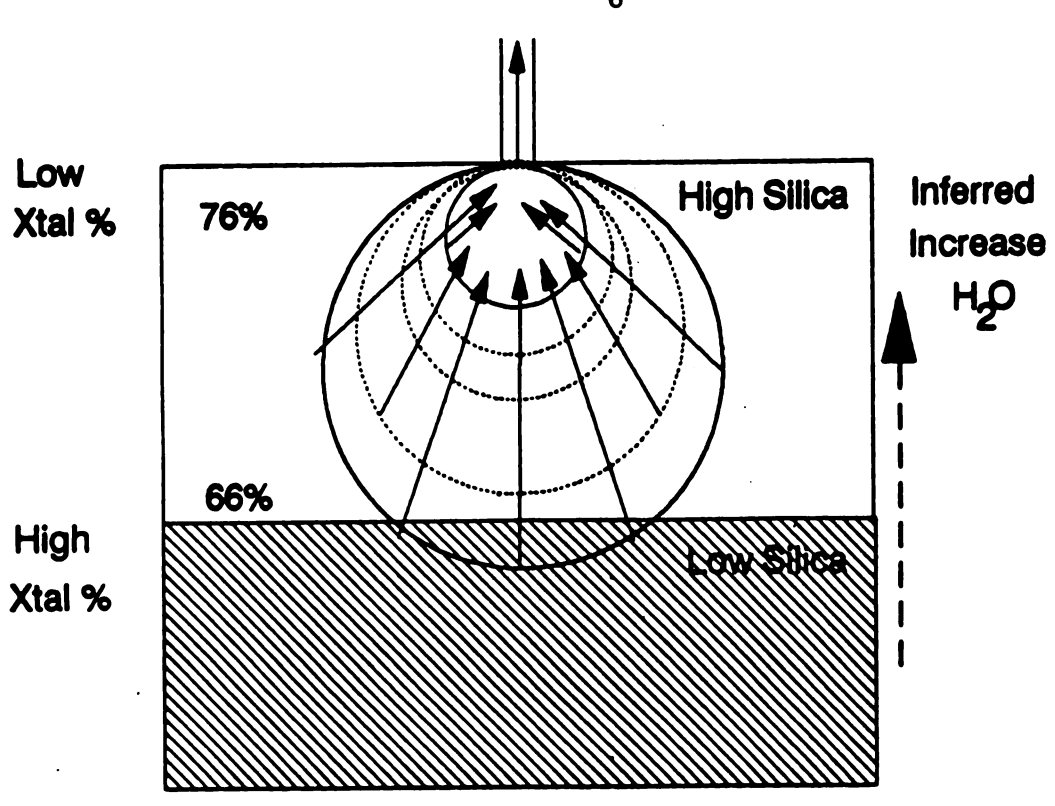


Figure 3. Schematic eruption dynamics of the Rainier Mesa ash-flow sheet.

silicic basal unit, and grading upward to more mafic compositions (Blake, 1981). Though the model presented here is a schematic oversimplification, the main ash-flow sheet of the Rainier Mesa Member is interpreted to have erupted generally in this manner (Mills, 1991). This type of eruptive sequence would indicate the tephra-fall deposits preceding the eruption of the main ash-flow sheet should tap predominately the uppermost portion of the magma body. Consequently, in a layered magma system such as the Rainier Mesa Member, the ash-fall deposits should consist of the most fractionated upper portion of the magma.

This study indicates that chemical variation and compositional distribution of the tephra-fall sequence beneath the Rainier Mesa Member are inconsistent with the above model. Furthermore, it is demonstrated that the large Rainier Mesa magma body probably was not present in its entirety at the time the tephra-fall deposits were erupted.

DESCRIPTION OF THE TEPHRA-FALL SEQUENCE

The tephra-fall sequence is well exposed at two locations on the Nevada Test Site (NTS). One section is located on the southwest side of Rainier Mesa, and the other is located on the south side of Pahute Mesa (Fig. 1). At both locations, the tephra-fall sequence unconformably overlies older deposits (Tiva Canyon Member on Rainier Mesa and the Grousse Canyon Member on Pahute Mesa (Fig. 4)). It is truncated above by the

		-
Alluvium	0-11 Ma	
Basalts		0-13 Ma
Stonewall Flat Tuff		6.5 Ma
Thirsty Canyon	Tuff	7.5 Ma
Rhyolite lavas of Shoshone Mountain		9.0 Ma
Mafic lavas		9-10 Ma
Timber	Ammonia Tanks	11.4 Ma
Mountain Tuff	Rainier Mesa	11.6 Ma
Rhyolite lavas of Fortymile Canyon		11-13 Ma
	Tiva Canyon	
Paintbrush	Yucca Mtn.	
Tuff	Pah Canyon	13 Ma
	Topopah Springs	
Wahmonie and Salyer formations		13.5 Ma
Crater Flat Tuff		13.5 Ma
Belted Range Tuff	Grousse Canyon	***
	Tub Springs	14 Ma
Dacite lavas and breccias		14 Ma
Lithic Ridge Tuff		14 Ma
Rhyolite of Kawich Valley		15 Ma
"Older" tuffs		15 Ma
Sanidine-rich tuff		15 Ma
Tuff of Yucca Flat		15 Ma
Redrock Valley	16 Ma	
		-

Figure 4. Generalized stratigraphy of major volcanic units of the Southwest Nevada Volcanic Field and approximate ages (after Byers et al., 1989).

basal surge deposit of the Rainier Mesa ash-flow sheet.

The tephra fall underlying the Rainier Mesa ash-flow sheet (Fig. 5) comprise a series of layered deposits that consist of sorted pumice layers and ash beds; and, unsorted, massive layers of pumice-rich ash often containing minor lithic and obsidian (i.e. non-vesiculated glass fragments).

Pumice-fall layers make up a large portion of the total tephra-fall unit. They consist of moderately to very well sorted light gray to brown pumice fragments. The individual pumice fragments range from sand-sized to cobble-sized clasts but are typically 0.5 to 10 cm in diameter. Pumice-fall layers are often well stratified and exhibit normal or reverse grading possibly due to changes in eruption velocity. They often contain minor amounts obsidian and lithic fragments.

Ash layers within the tephra-fall sequence typically range in thickness from approximately 0.25 cm to about 4 m. They are light- to medium-gray or light- to medium-brown in color. Medium grained layers of glass fragments containing abundant lithic fragments are commonly included in the tephrafall deposits. As with all tephra-fall deposits, the texture and particle composition is dictated by gravity, wind, and eruption velocity (Cas and Wright, 1987).

Interbedded with the tephra-fall layers are numerous, very poorly sorted, unstratified, discontinuous layers of pumice and lithic fragments in an ash matrix (Fig. 6). They commonly pinch and swell and exhibit flow



Figure 5. Tephra-fall sequence underlying the Rainier Mesa ash-flow sheet (Pahute Mesa location).





Figure 6. a.) Small ash-flow layer within the tephra-fall sequence. b.) $52\ m$ ash flow within the tephra-fall sequence (Pahute Mesa location).

characteristics such as flow casts and basal zones of reworked material, typically 2-5 cm in thickness, presumably ripped up from the underlying layer. These layers have been interpreted by Warren and Valentine (1990), as small ash-flow layers. Lithic fragments typically constitute only a minor portion of these layers. The small ash-flow layers also occasionally contain plant root remains in the top few centimeters. The most noticeable characteristic of these small ash-flow layers is the color change that each layer exhibits from base to top (Fig. 6). Each small ash-flow layer grades from basal white (or light gray), upward to brown. Typically, the ash matrix and small pumice fragments change color, while the larger pumices (>1.5 cm) remain white or light gray throughout an individual layer.

A channel cut is present in section on Pahute Mesa. The cut is approximately 2 m across, and 3 m deep with steep walls. It is filled with very poorly sorted gray ash and pumice deposits, and unconformably overlain by a pumice-fall layer.

Also included in this section is a 52 m thick ash-flow layer. Unlike the abundant small zoned ash-flow layers, this thick layer exhibits no change in color from base to top. There is a 0.3 m surge deposit of white ash at the base, overlain by an additional 51.7 m of fine white ash matrix containing boulder-sized lithic and pumice fragments (up to 50 and 20 cm respectively) (Fig. 6). Though this deposit is

thick, it is not laterally traceable indicating that the flow most likely fills a localized channel or depression.

SAMPLE SELECTION AND PREPARATION

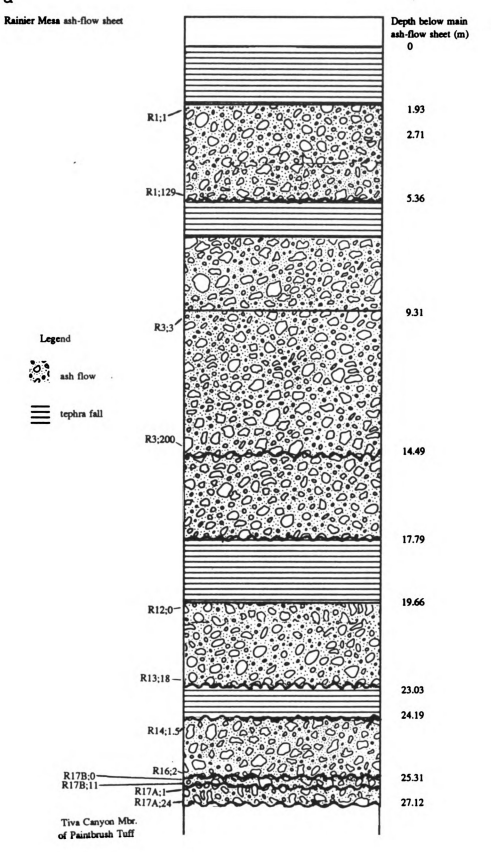
Because of the excellent exposure and stratigraphic control, samples for this study were collected extensively from the two well-exposed sections on Pahute Mesa and Rainier Mesa. Figure 7 illustrates the stratigraphic positions from which glassy pumice and whole-rock samples were collected.

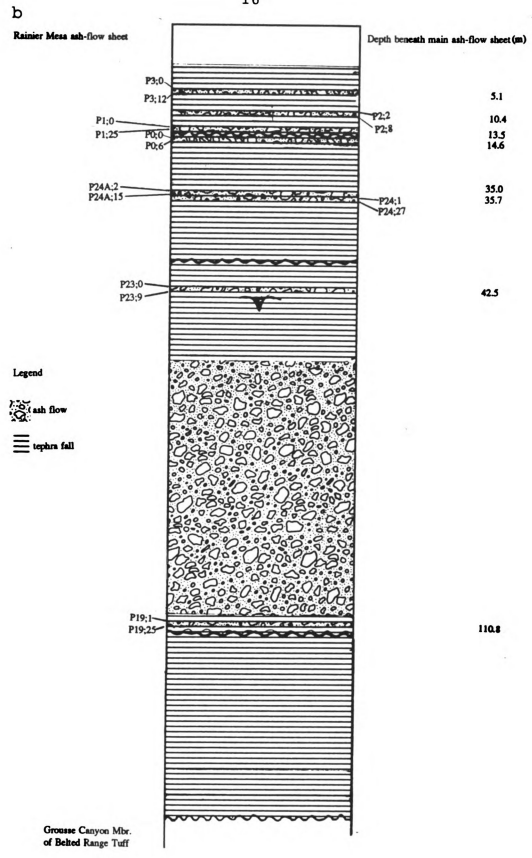
In general, glassy pumice fragments are better indicators of chemical processes taking place within magma bodies than whole-rock samples (Hildreth and Mahood, 1985; Flood, et al., 1989; Schuraytz, et al., 1989; Vogel, et al., 1989; Mills, 1991). Glassy pumice fragments represent solidified packets of the liquid and crystal portions of the magma being erupted from a vent at a given instant in time (Flood, 1989). Whole-rock samples represent an average composition of material being deposited from an eruption over a given period of time. For this reason, glassy pumices fragments were collected for analysis from the entire tephra-fall sequence to ensure representation of the entire chemical variation of the sequence.

The small ash-flow layers within the tephra-fall sequence, however, often did not contain pumice fragments large enough for analysis. In fact, even when the small ash-flow layers did contain pumice fragments large enough for

Figure 7. Generalized stratigraphic column of the tephra-fall sequence at a). Rainier Mesa location and b.) Pahute Mesa location. Samples collected from the bottom and the top of each small ash-flow are labelled. The depth of each sampled layer beneath the overlying main ash-flow sheet is also shown.







analysis, they did not reflect the same degree of color change from the bottom to the top of the layer as did the ashy matrix. In these cases whole-rock samples were collected, across the color change from the top to the bottom of each small ash-flow layer.

Determination of the chemical variation among the different layers was also a priority. To achieve this, representative small ash-flow layers from the entire tephrafall sequence were sampled.

Altogether, more than one hundred glassy pumice fragments, previously collected by John Brannon (personal communication, 1988), and 77 whole-rock samples from 14 small ash-flow layers within the tephra-fall sequence were analyzed for major and trace element abundances (Appendix 1).

Major and trace element analyses of Cr, Ni, Cu, Zn, Rb, Sr, Y, Zr, Nb, La, and Ba, were obtained using X-ray fluorescence (XRF) methods described by Mills (1991). U.S. Geological Survey (USGS) whole rock standards run both as known and unknown concentrations were used as a means of measuring the error of analysis. For XRF analyses, whole rock standard errors of less than or equal to 1% were accepted with the following exceptions. Cr, Ni, and Cu concentrations were generally below XRF detection limits. Errors of La and Ba were generally greater than 10 ppm, however these two trace elements were also analyzed for, using instrumental neutron activation analysis (INAA).

Additional trace element and selected rare earth element (REE) abundances were obtained from 35 samples (Appendix 1) using INAA methodology also described by Mills (1991). Associated errors are reported in Appendix 2.

Samples for INAA were chosen from small ash-flow layers within the tephra-fall sequence. Samples were selected which stratigraphically represented layers throughout the tephra-fall sequence and also displayed significant chemical variation based on XRF analyses.

Prior to analysis of whole-rock samples,
lithic fragments large enough to be identified with the
unaided eye were removed.

This study focuses on both the tephra fall and the small ash-flow layers comprising the tephra-fall sequence. For clarity, the term tephra-fall sequence is used when referring to the sequence as a whole. Tephra fall refers to deposits that were erupted into the air and subsequently deposited. In addition, small ash-flow layers refer to the ash-flow deposits contained within the tephra-fall sequence, whereas main ash-flow sheet or Rainier Mesa ash-flow sheet refers to the voluminous (1200 km³) caldera-forming ash flow that overlies the tephra-fall sequence.

MAJOR ELEMENT VARIATION

Major and trace element analyses were performed on 116 pumice fragments and 77 whole-rock samples collected from two

stratigraphic sections of the tephra-fall sequence beneath the Rainier Mesa ash-flow sheet. In each case, the chemical range obtained from the pumice samples was nearly the same as that of the whole-rock samples for the two sections (Appendix 1). Typically, chemical trends defined by the whole-rock samples often possess slightly less variation than individual pumices. This effect is due to the fact that because whole-rock samples are an average composition, some of the variation is masked.

Figure 8 illustrates major element variation plotted against SiO₂, normalized to 100%, for whole-rock samples from each section. Major element variation of the overlying Rainier Mesa ash-flow sheet (Mills, 1991) is also shown for comparison. (Analyses of individual pumice fragments are listed in appendix 1). In all cases, the tephra-fall analyses occur within the high-silica portion of the Rainier Mesa ash-flow sheet.

Within the tephra-fall deposits, all of the major element abundances decrease with increasing silica. The overlying Rainier Mesa ash-flow sheet is characterized by points of inflection within the TiO_2 , FeO, MgO, Al_2O_3 , Na_2O , and trends at approximately 65% SiO_2 . This may be due to the removal of phenocryst phases (Mills, 1991), however, because of their mobility in glassy pumice fragments, this interpretation for the alkalies may be tenuous. The total silica range of the tephra-fall sequence underlying the Rainier Mesa ash-flow sheet is about 67% to 78% SiO_2 -- nearly the entire range of

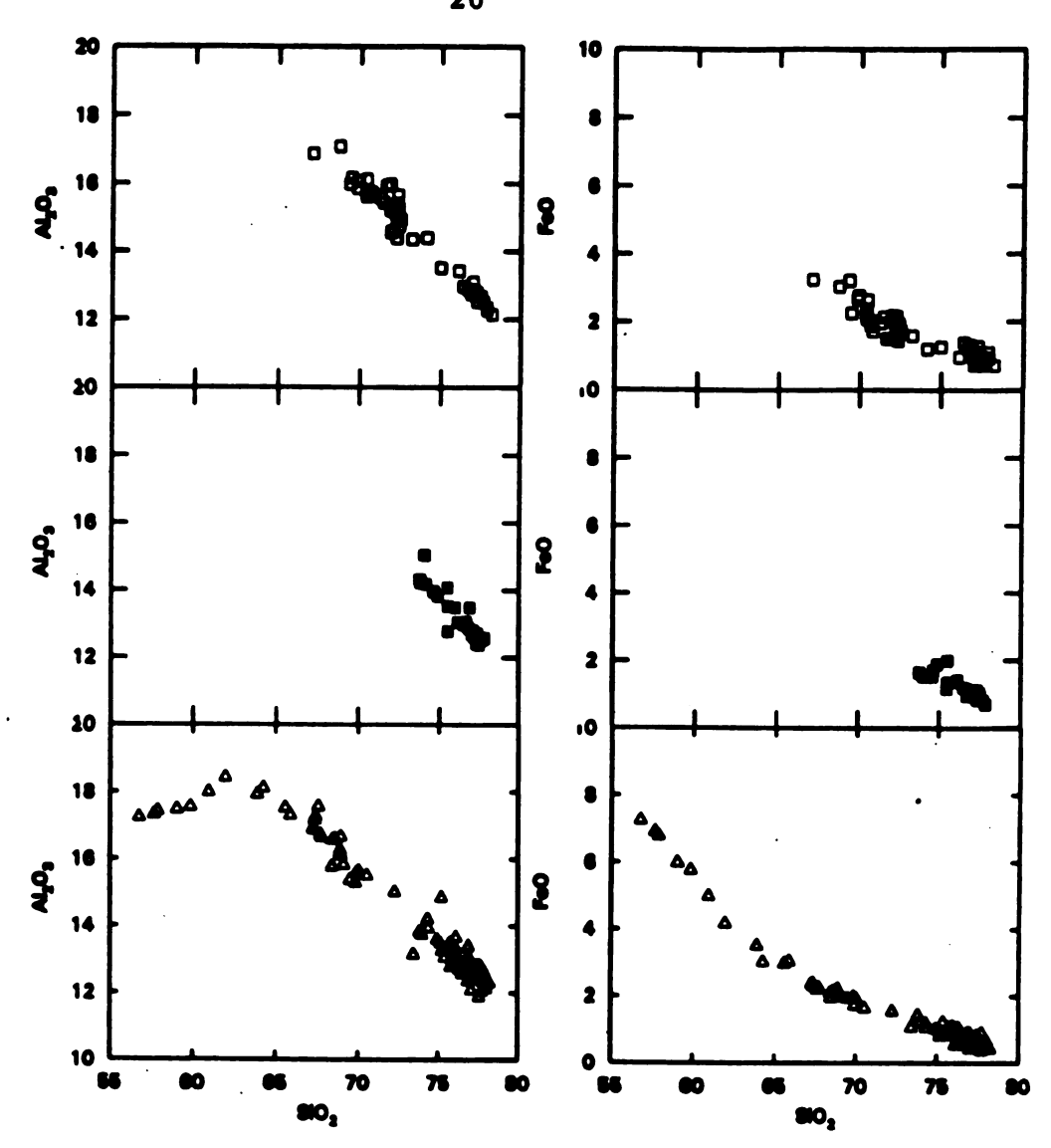


Figure 8. Major element variation of small ash-flow layers within the tephra-fall sequence and the overlying Rainier Mesa ash-flow sheet. Open squares = Rainier Mesa location; Solid squares = Pahute Mesa location; Open triangles = Main ash-flow sheet.

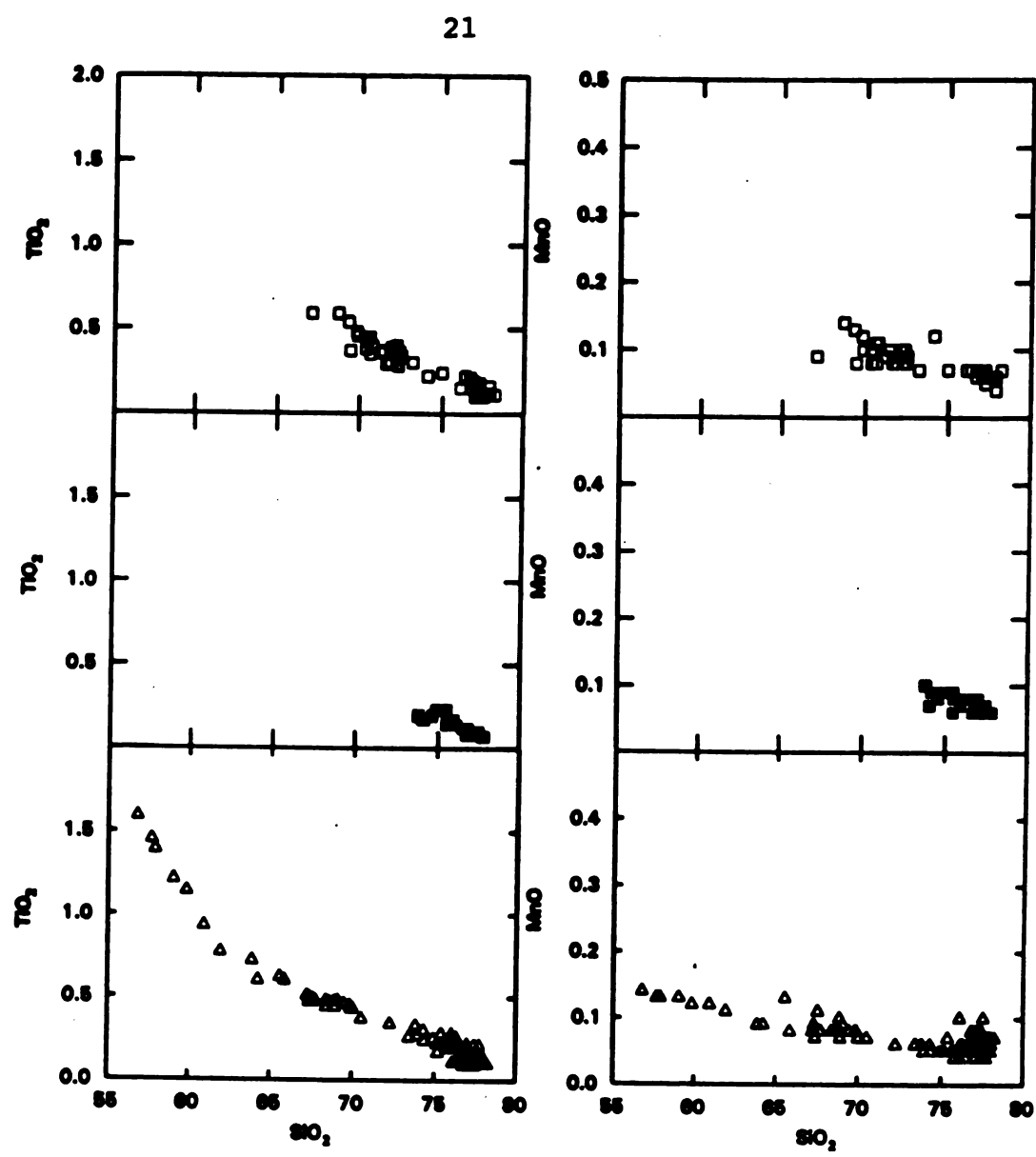


Figure 8 (continued).

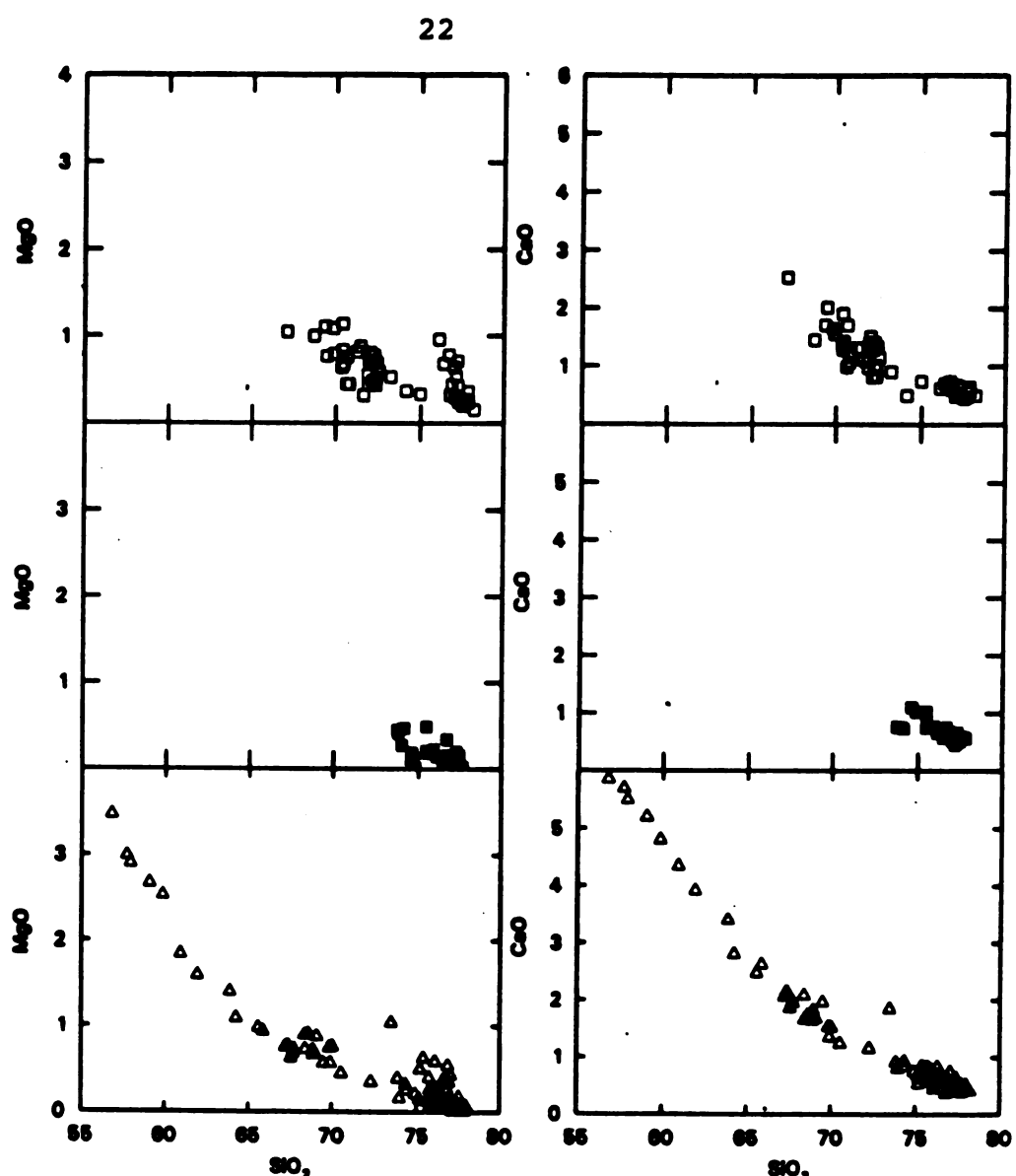


Figure 8 (continued).

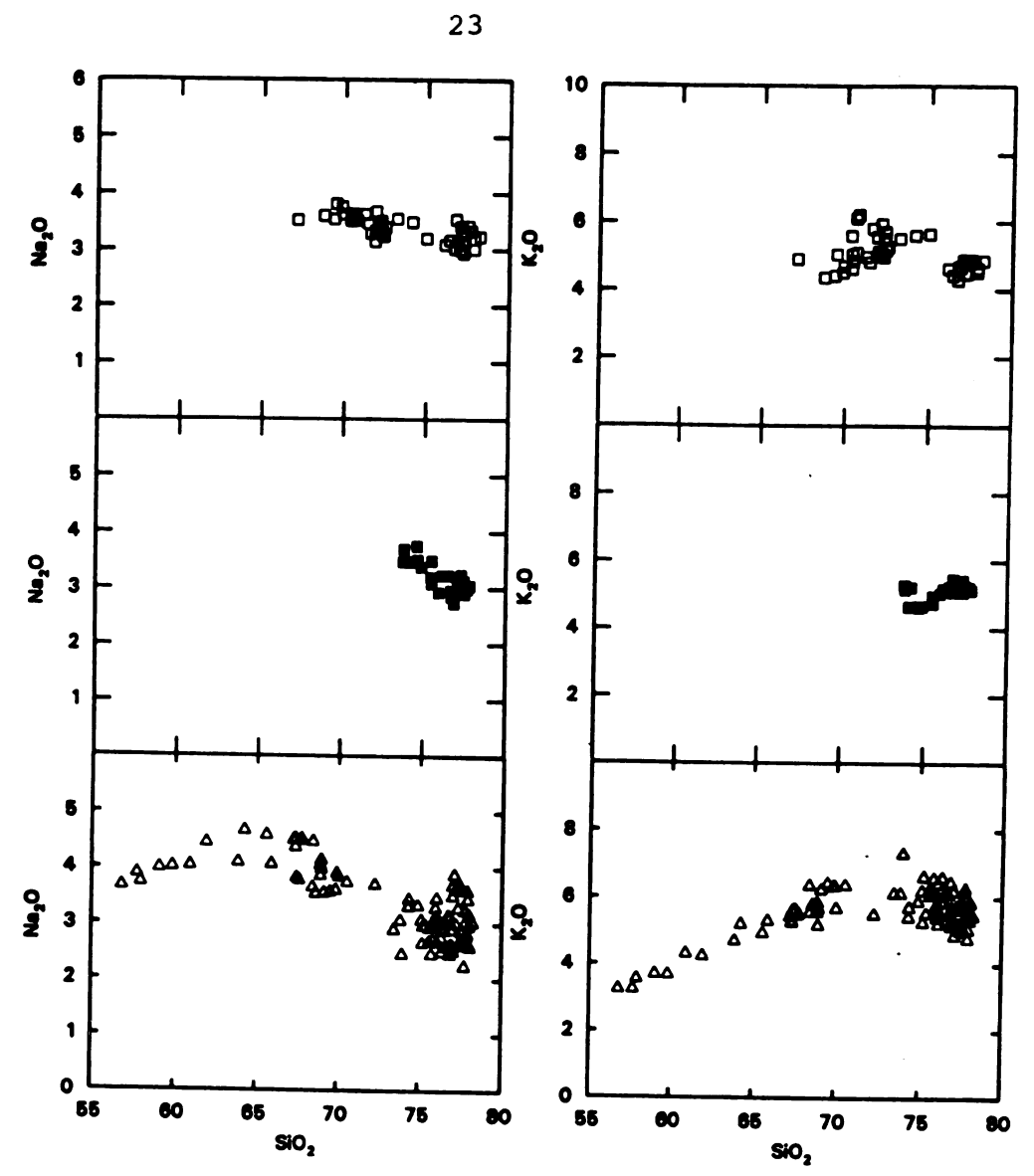


Figure 8 (continued).

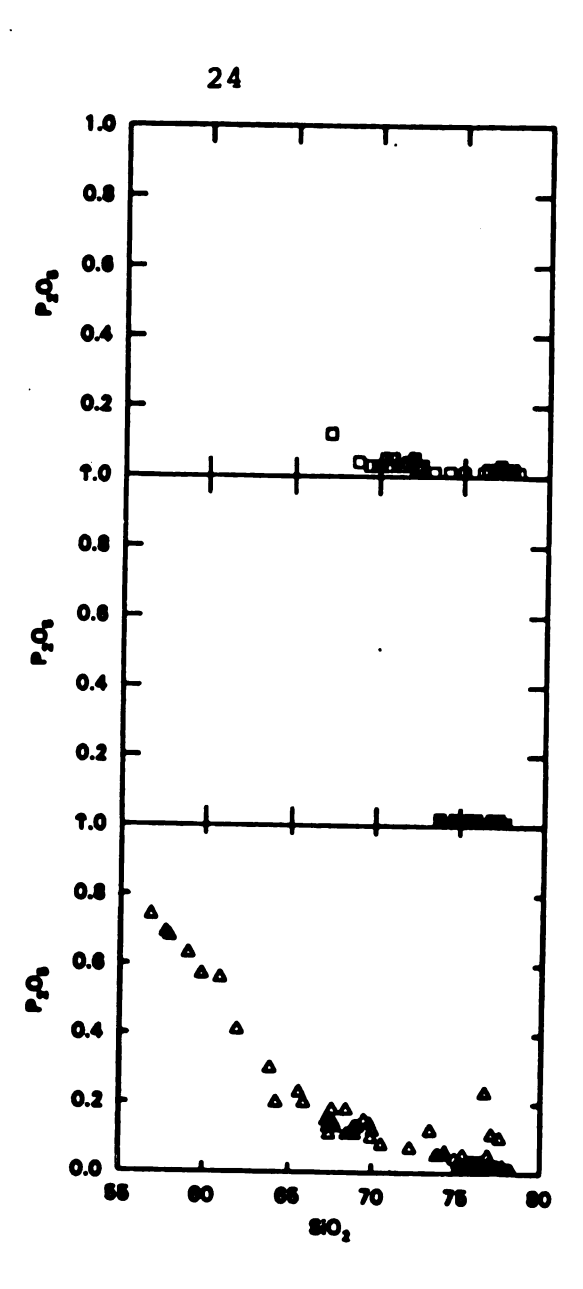


Figure 8 (continued).

the high-silica portion of the Rainier Mesa ash-flow sheet.

Similarly, the chemical ranges of Al_2O_3 (12-17.5%), FeO (0.5-3.5%), MgO (0.1-1.1%), and CaO (0.5-2.75%) of the tephrafall sequence, as well as the other major oxides, are characterized by significant chemical variation -- virtually equivalent to that of the entire high-silica portion of the overlying Rainier Mesa ash-flow sheet.

TRACE ELEMENT VARIATION

Trace element variation of the tephra-fall sequence is also very similar to the high-silica portion of the overlying Rainier Mesa ash-flow sheet. This may indicate that processes controlling trace element distribution in the tephra-fall sequence and in the Rainier Mesa ash-flow sheet are the same.

Trace element abundances for the small ash-flow layers within each tephra-fall section are expressed relative to SiO₂ in Figure 9. Trace element variation of the overlying Rainier Mesa ash-flow sheet is shown for comparison (Mills, 1991). Of the analyzed trace elements for the tephra-fall sequence, only Rb shows clear enrichment with increasing silica. The remaining trace elements either decrease with increasing silica, have constant concentrations, or do not display well defined trends due to scatter. Th is characterized by large variation (10-30 ppm) at nearly constant silica (75-78% SiO₂). Large variation (approximately 11 to 40 ppm Th) has also been reported for the Rainier Mesa ash-flow sheet at nearly

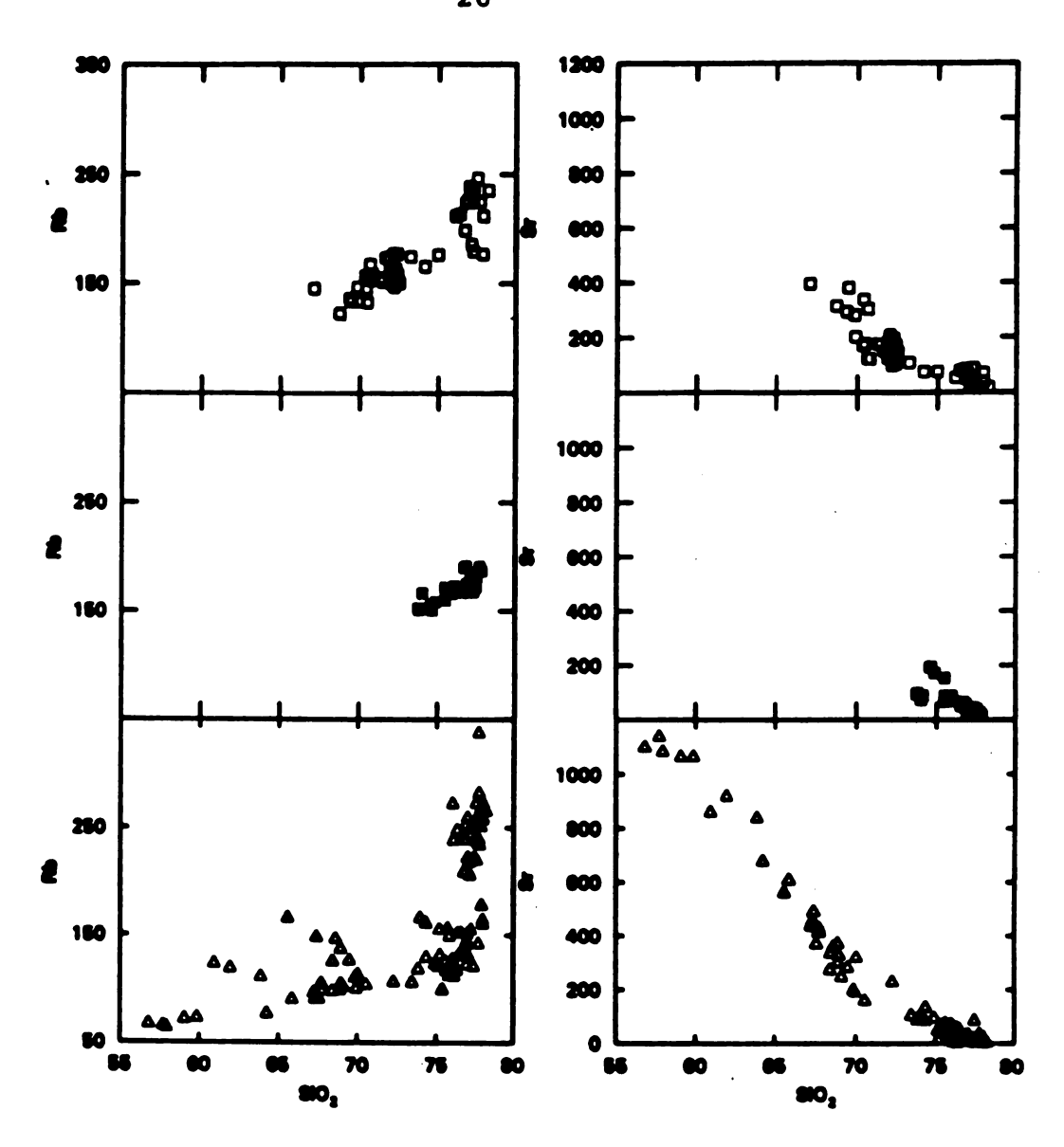


Figure 9. Trace element variation of small ash-flow layers within the tephra-fall sequence and the overlying Rainier Mesa ash-flow sheet. Symbols are the same as in Figure 8.

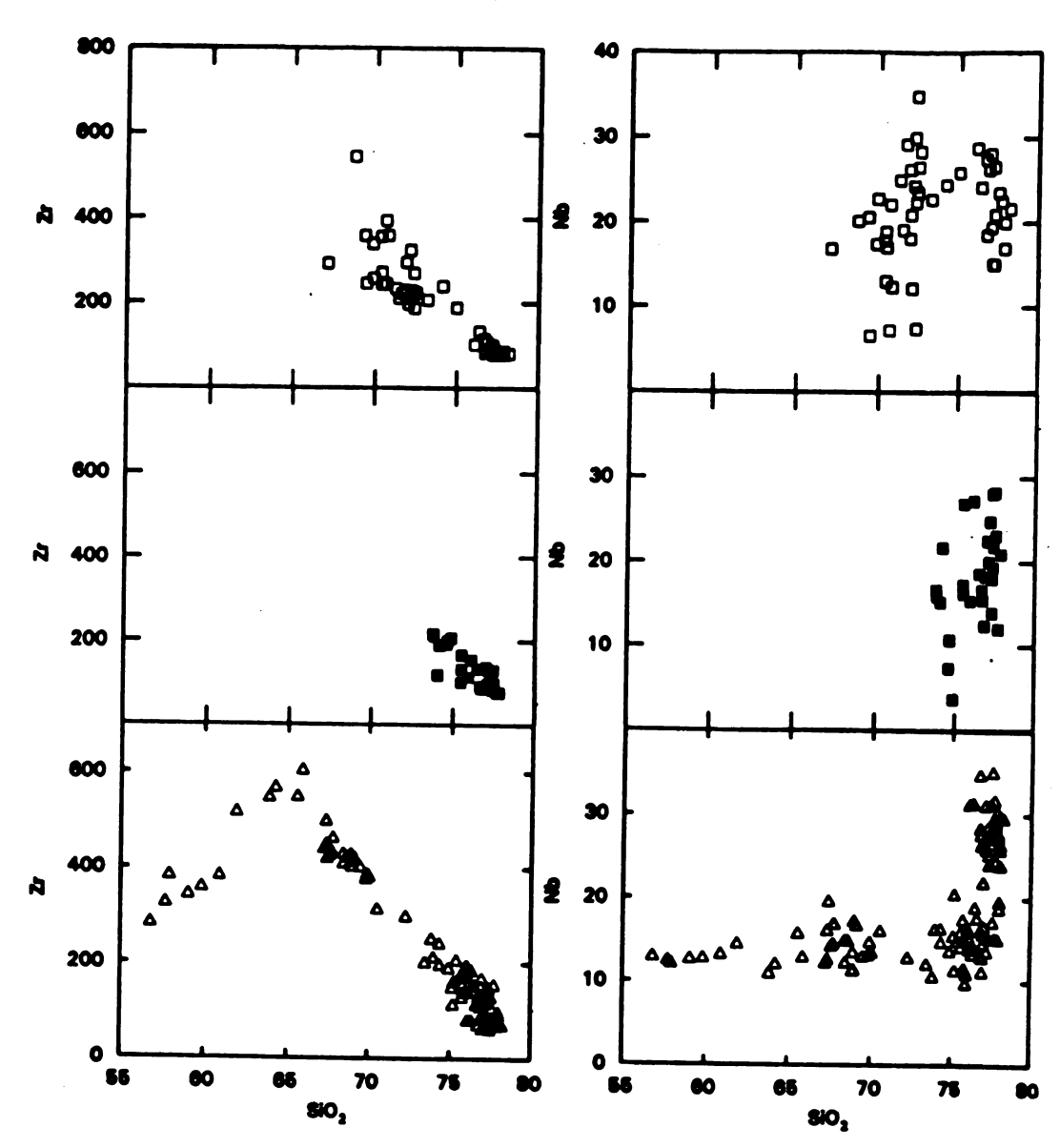


Figure 9 (continued).

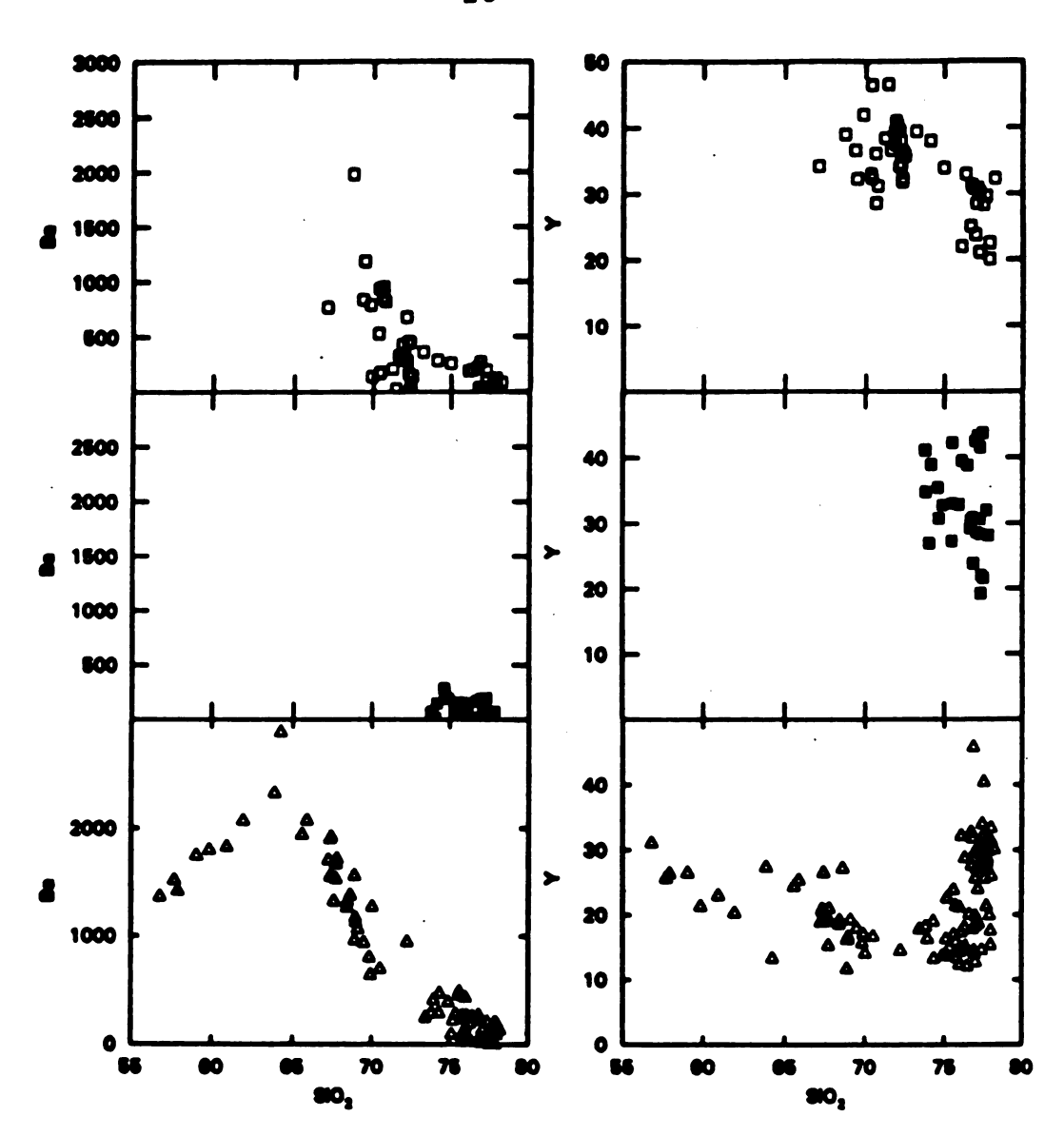


Figure 9 (continued).

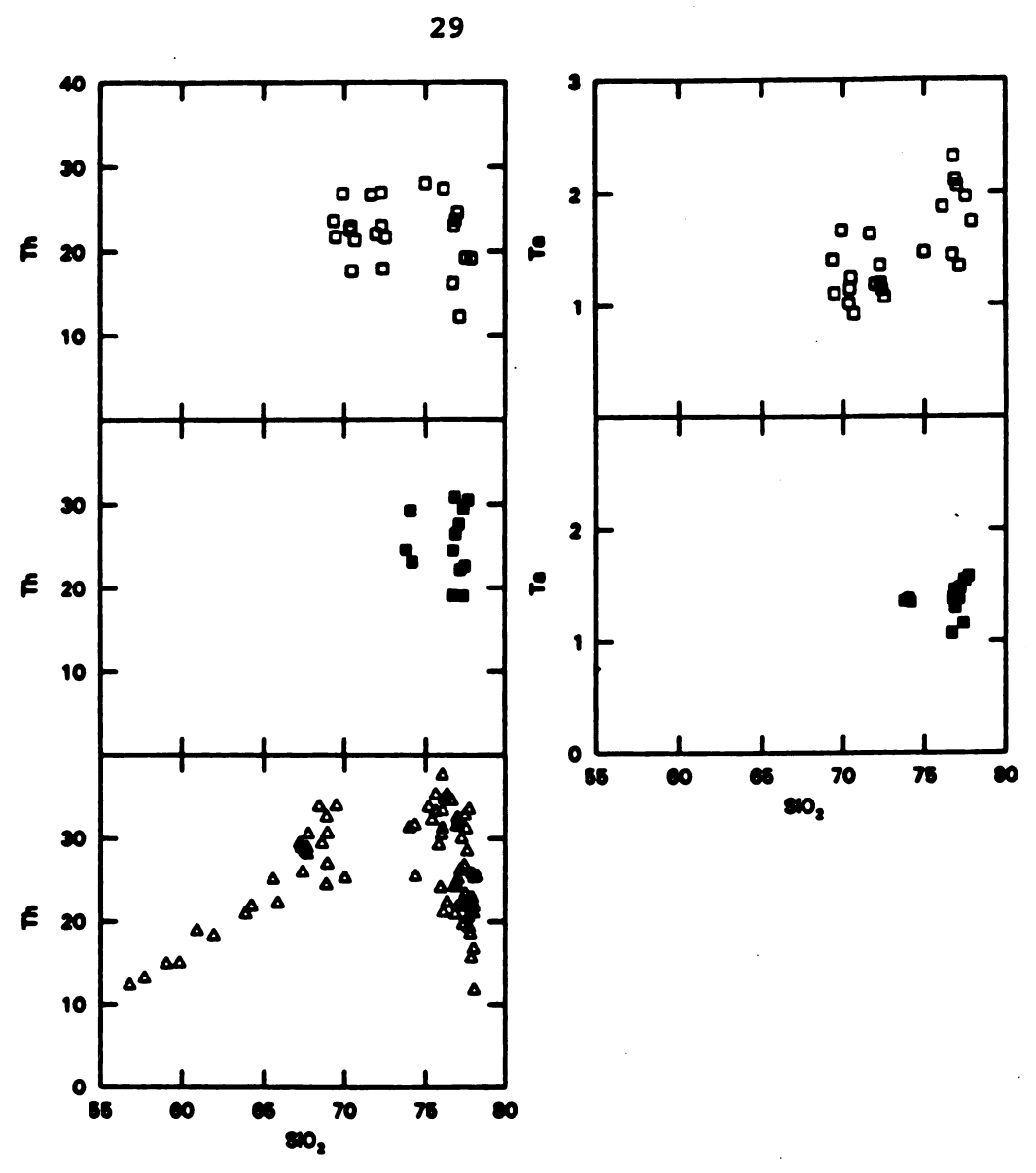


Figure 9 (continued).

constant silica (Mills, 1991). Significant Th variation at constant silica has been accounted for in the Rainier Mesa Member by the existence discrete magma packets being erupted simultaneously from the Rainier Mesa magma body (Mills and Vogel, personal communication, 1992).

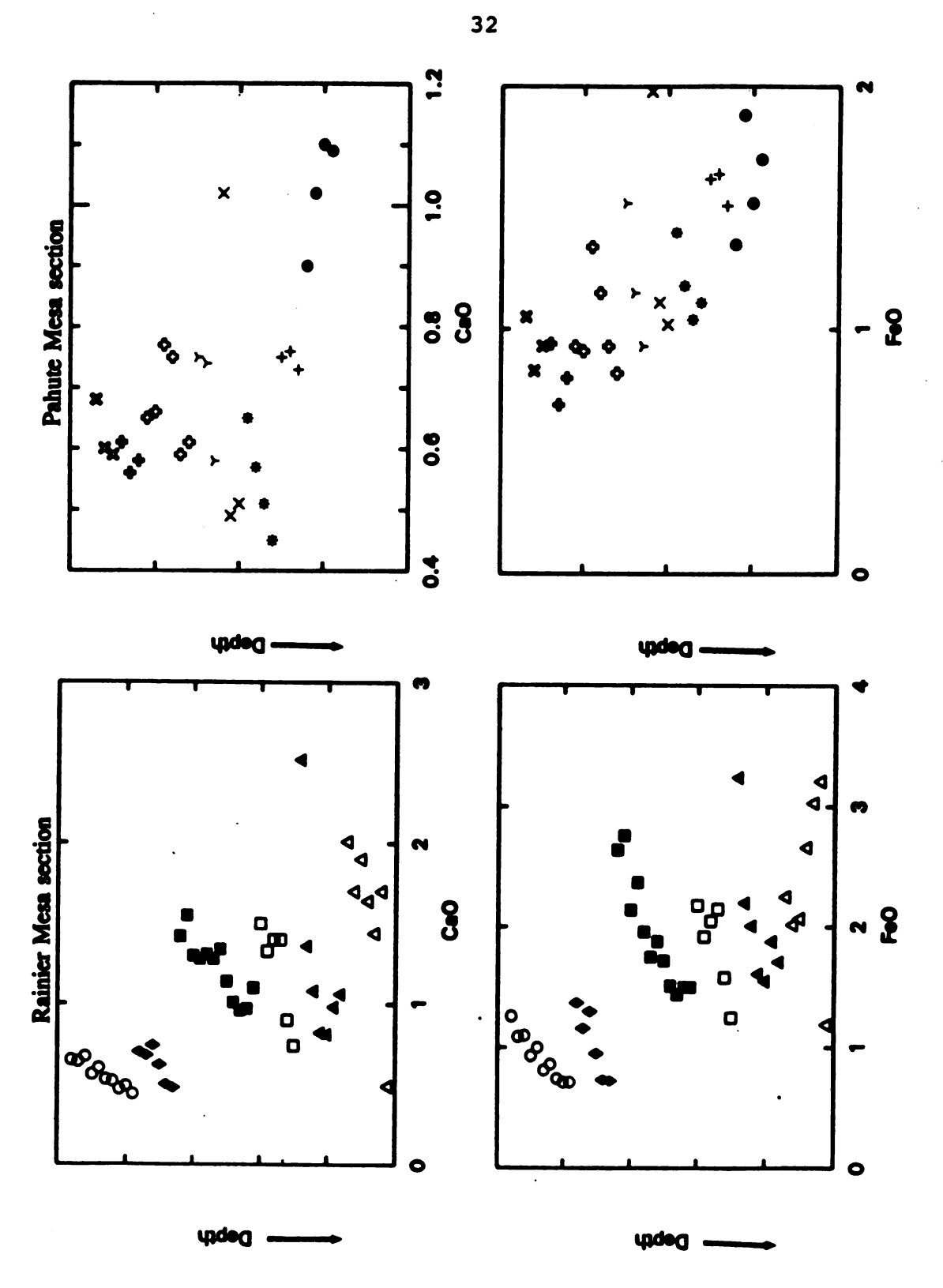
CHEMICAL VARIATION WITH STRATIGRAPHIC POSITION

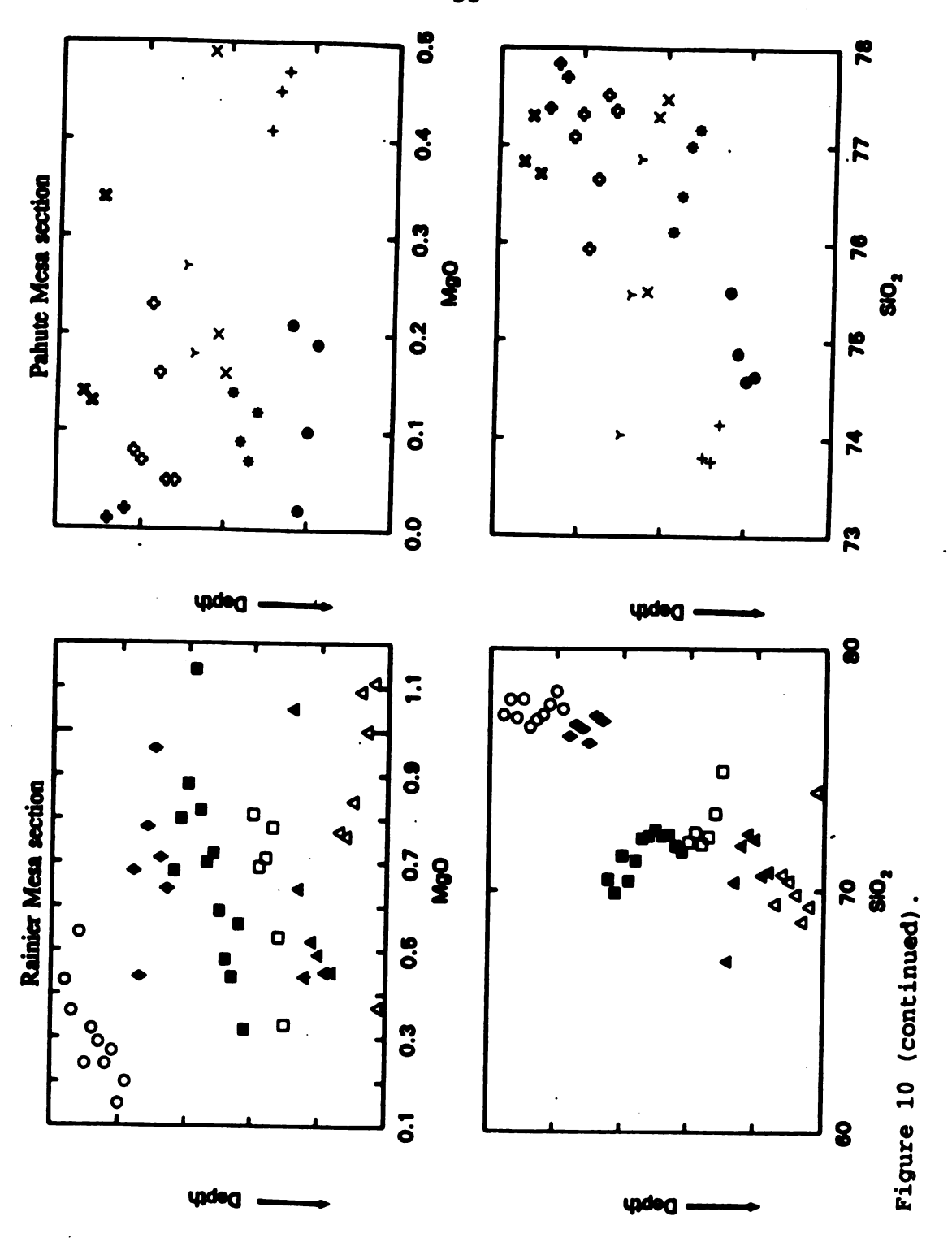
Because the tephra-fall deposits should be inversely related to the composition of the magma body from which they were erupted (see Figure 3), it is useful to plot elemental abundance against relative stratigraphic position (i.e. depth from the base of the Rainier Mesa ash-flow sheet) of each small ash-flow layer within the tephra-fall sequence.

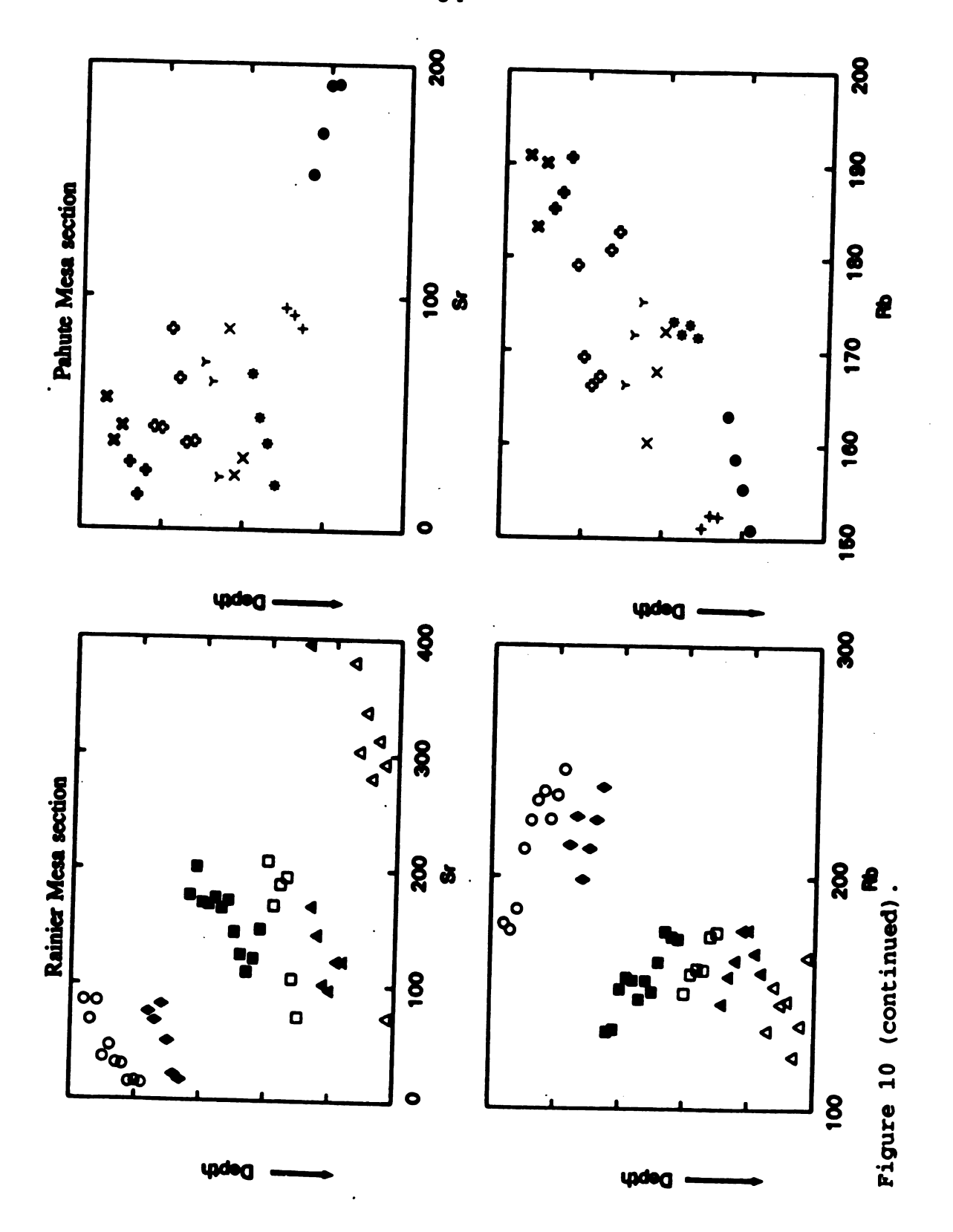
In Figure 10, major and trace element abundances are plotted against stratigraphic position of the tephra-fall deposits, expressed as relative depth, so that the chemical variation may be inspected as a function of relative time of eruption. There are two major observations that are important in this figure.

The first major observation is that each small ash-flow layer (expressed as a different plot symbol) exhibits a distinct trend when plotted against its relative stratigraphic position (expressed as relative depth) within the sampled section. This trend typically progresses from a more evolved magma at the base to a less evolved magma toward the top of each layer (e.g. in the diagram of FeO vs. relative depth, the

Figure 10. Major and trace element variation with stratigraphic position (depth), for small ash-flow layers within the tephra-fall sequence. Each plot symbol denotes a separate small ash flow within the sequence.







sample with the lowest FeO concentration in each layer is located at the bottom of the flow). This within-layer trend is more distinct in the Rainier Mesa section than in the Pahute Mesa section.

The difference in the two sections is the result of greater sampling density from the Rainier Mesa section. In the Rainier Mesa section, thicker layers are present, and generally more samples were collected per layer than from Pahute Mesa. Many layers from the Pahute Mesa section, however, are still characterized by this within-layer trend.

Interestingly, the small ash-flow layers from Rainier Mesa thicken towards to top of the section while their chemical variation decreases. For example, there is an increase in total FeO from 1.3 to 3.3 wt.% in the small ash-flow layer at the base of this section. This increase occurs over a vertical thickness of less than one meter. However, the uppermost layer exhibits in increase from only 0.75 to 1.3 wt.% over a vertical thickness of about 5 meters (Fig. 10).

The second major observation is that there is a larger scale trend of the entire tephra-fall sequence. This trend is opposite that of each individual layer (that is, the small ash-flow layers become increasingly evolved toward the top of each section).

Trace element patterns relative to depth within and among small ash-flow layers within the tephra-fall sequence follow patterns similar to those of the major oxides. The small ash-

flow layers within the tephra-fall sequence are chemically zoned with respect to trace elements. As with the major elements, these trace elements produce a within-layer trend of decreased magmatic evolution toward the top of each small ashflow layer. In addition to the within-layer trace element behavior is a larger scale trend from layer to layer. This is one of increasing magmatic evolution towards the top of the section.

RARE EARTH ELEMENT VARIATION

Chondrite normalized Rare Earth Element (REE) concentrations for the small ash-flow layers from each section are plotted in Figure 11. REE concentrations for the overlying Rainier Mesa ash-flow sheet are shown for comparison (Mills, 1991). As with major and trace element abundances, the REE variation of the tephra-fall sequence is similar to that of the high-silica portion of the overlying Rainier Mesa ash-flow sheet. With the exception of the heavy rare earth elements, the variation of the small ash-flow layers within the tephra-fall sequence is as variable as the high-silica portion of the Rainier Mesa ash-flow sheet. This may be an artifact of the small number of samples from the tephra-fall sequence for which REEs were analyzed. Another possibility may be that there was assimilation of the surrounding wall rock, or addition of another magma after the eruption of the tephra fall but prior to caldera collapse. Gaps in the REE

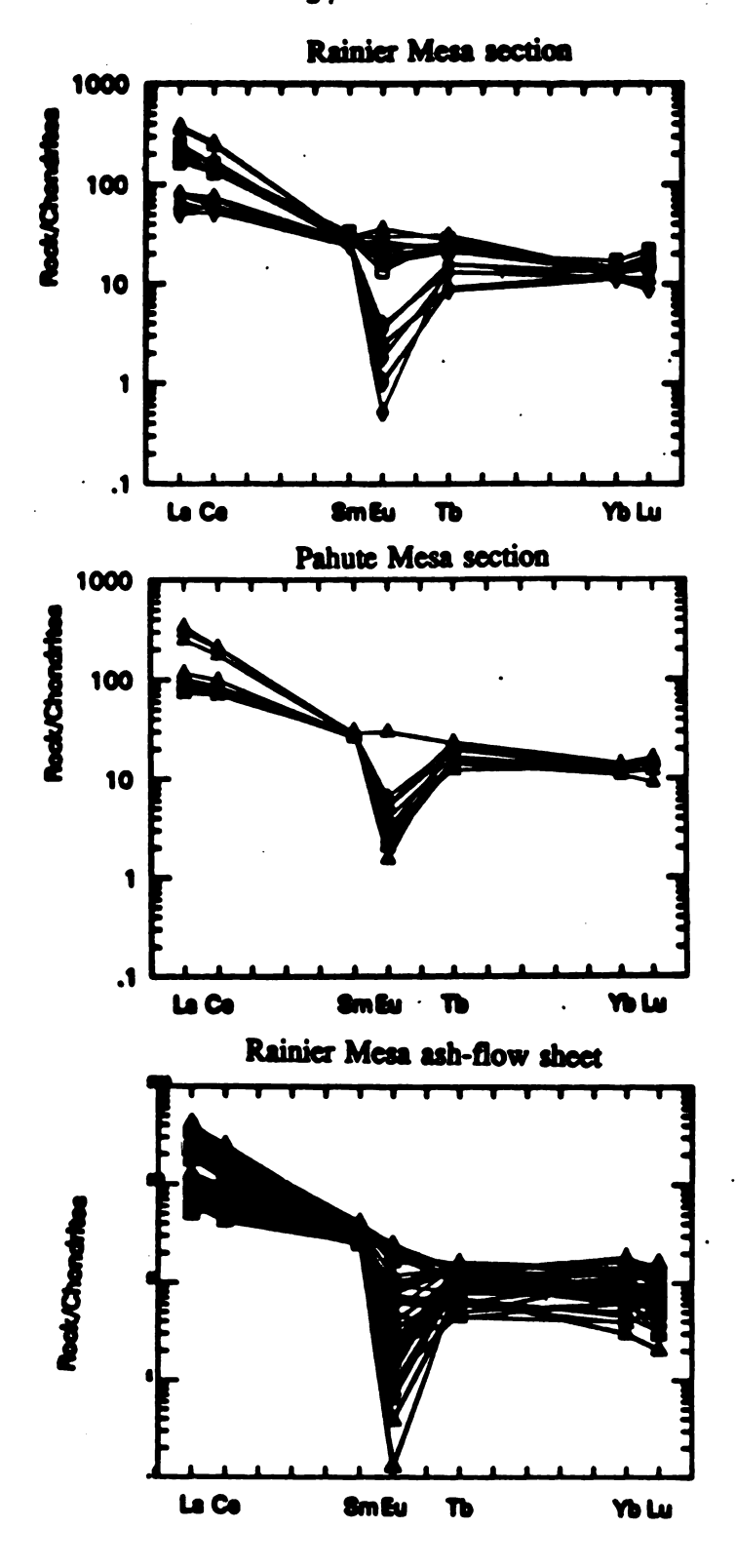
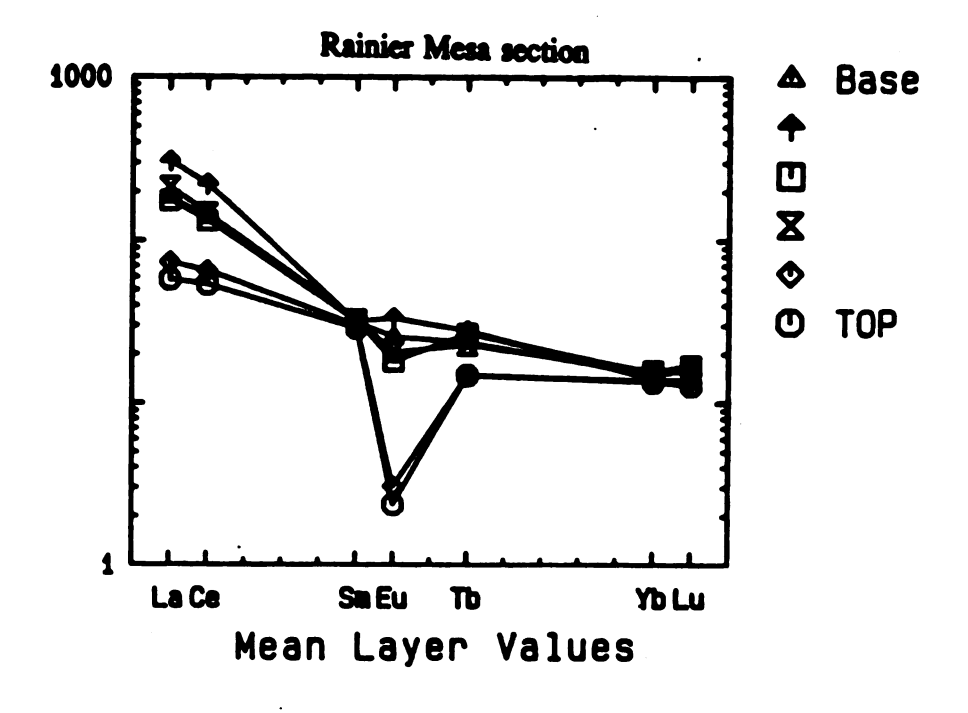


Figure 11. Chondrite normalized REE patterns for small ashflow layers within the tephra-fall sequence and the high-silica portion of the Rainier Mesa ash-flow sheet.



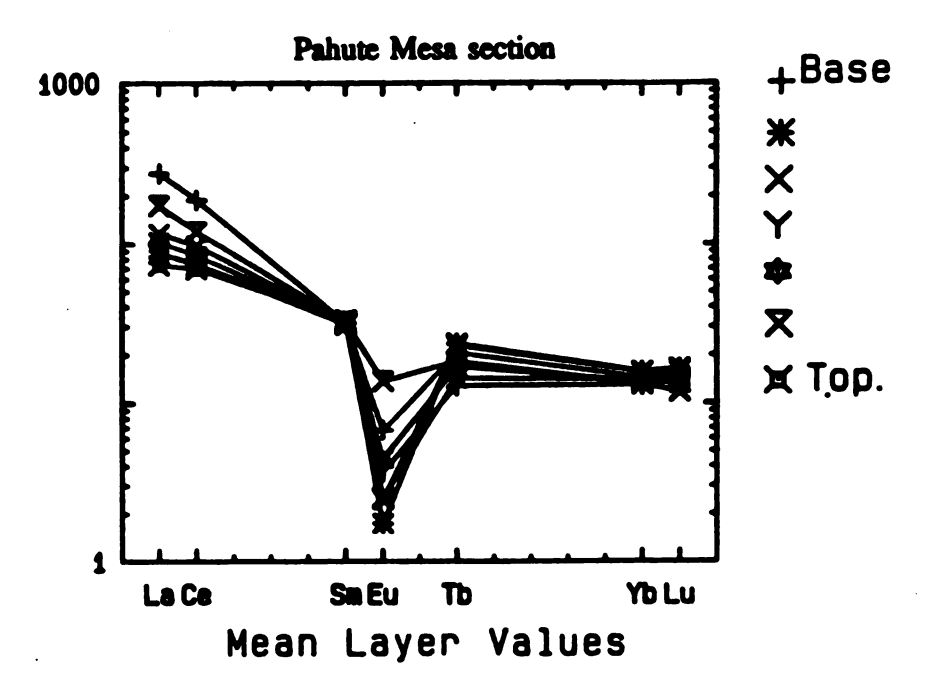


Figure 12. Average REE abundances for small ash-flow layers within the tephra-fall sequence.

data is a function of sample selection (see section on sample selection and preparation).

The REE relationship among the small ash-flow layers are plotted in Figure 12. The mean rare earth elemental values for each layer are plotted to illustrate the change in average layer concentrations among the different ash-flow layers from the bottom to the top of the tephra-fall sequence. The first erupted layers are relatively LREE and Eu enriched, and become increasingly depleted with each subsequently erupted ash-flow layer. This is the same overall trend observed for the major and trace elements with depth. That is, the layers become increasingly evolved upsection.

DISCUSSION

This study indicates that in the case of the Rainier Mesa ash-flow sheet, the associated tephra-fall deposits are essential for interpreting development of the large magma body. Two lines of evidence indicate that the tephra-fall deposits underlying the 1200 km³ Rainier Mesa ash-flow sheet could not have been erupted from the uppermost fractionated portion of a large, chemically zoned, magma body. First, the variation of the tephra-fall sequence is chemically equivalent to the entire high-silica portion of the overlying Rainier Mesa ash-flow sheet. This high-silica portion of the ash-flow sheet makes up about 90% of this voluminous (1200 km³) deposit. Because the tephra-fall deposits represent a very

small volume, it would be highly unlikely for the observed range of chemical composition of the tephra-fall sequence to be present if it were erupted from only the uppermost fractionated portion of the very large volume Rainier Mesa magma body. This conclusion is stronger if one considers that the tephra-fall sequence was not produced by a single continuous eruption, but rather a series of very small eruptions.

Secondly, each small ash-flow layer within the tephrafall sequence is also characterized by significant chemical variation. The volume of one of these ash-flow layers is negligible (probably less than 0.01 km³) compared to that of the entire Rainier Mesa ash-flow sheet (1200 km³). With this in mind, it would be extremely difficult to produce the observed chemical variation in these layers by periodic eruption from the uppermost fractionated portion of a very large magma body.

The possibility that each of the small ash-flow layers could have been erupted from deeper levels of the large-volume Rainier Mesa magma body (i.e. the classical eruption dynamics are incorrect) is disproved by the trend of a increased chemical evolution towards the top of the section. There is no reasonable way by which the within-layer trend and the opposing among-layer trend could be achieved if the small ash-flow layers were erupted from a very large-volume (>1200 km³) Rainier Mesa magma-body.

The evidence presented indicates that a large volume Rainier Mesa magma body was not likely to have been present throughout eruption of the tephra fall. The following model is one possibility for the origin of this tephra-fall sequence. In any model for the origin of these deposits, the following observations must be accounted for:

- 1.) The tephra-fall sequence is chemically equivalent to the entire high-silica trend of the overlying Rainier Mesa ash-flow sheet.
- 2.) Small ash-flow layers present within the tephra-fall sequence indicate numerous separate eruptions during the time of deposition of the tephra-fall sequence.
- 3.) Each small ash-flow layer within the tephrafall sequence is characterized by an upward chemical change from the base to the top of the layer. This change is one of a more silicic base grading upward to a more mafic top.
- 4.) The entire sequence is characterized by a more mafic component at the base of each section, which grades upward to a more silicic component at the top.

The fact that the tephra-fall is chemically equivalent to the high-silica portion of the Rainier Mesa ash-flow sheet, strongly suggests that the tephra fall belongs to the same petrologic system as the large Rainier Mesa ash-flow sheet. The presence of discrete numerous small ash-flow layers and evidence of plant growth between layers suggests there was some period of guiescence between ash-flow eruptions.

Because each small ash-flow layer is compositionally zoned, it is reasonable to assume that they erupted from a compositionally zoned magma body. The magma body would have to be small (or thin) in order to account for the degree of variation observed in these layers. Large-scale compositional variation among the ash-flow layers is consistent with periodic eruption from a continually evolving magma body.

The discontinuity of the small ash-flow layers suggests that a separate vent erupted each of the tephra-fall sections. They indicate that the ash-flows probably did not flow far from their source.

The most probable model for the evolution of the magma body is a situation where the large-volume Rainier Mesa magma body is produced by a small, thin, tabular, shallow, chemically zoned magma body that incrementally grew larger with time and periodically erupted, producing small ash-flow layers that are, in essence, "snapshots" of the magma body's evolution. Because the section from Rainier Mesa contains the least evolved small ash-flow layers, the magma body only

needed to initially exist beneath it. This magma body ranged from at least 67 to 74% silica (the silica variation of the stratigraphically lowest ash-flow layer in the Rainier Mesa section); and eruption from this small (or thin) magma body produced the first small chemically zoned ash-flow layer (Fig. 13a). The next, slightly more chemically evolved small ash-flow layer would have been erupted after recharge, growth, and differentiation of this small initial magma body.

The tephra-fall section from Pahute Mesa possesses less chemical variation than the Rainier Mesa section (Figs. 8 and For example, the silica content from the Rainier Mesa location ranges from 67 to 78%, whereas the silica content from the Pahute Mesa location ranges only from about 74-78%. Because of this constraint, the small ash-flow layers from Pahute Mesa are not required to erupt until the magma body evolved to a silica content of 74-75.5% (the silica range of the first erupted small ash-flow layer from the Pahute Mesa location) (Fig. 13b). When these small ash-flow layers were erupted, the magma body must have been at least 10 km wide in order to underlie both tephra-fall sections (Fig. 1). At this time the entire magma body ranged in silica from at least 67% (the lowest silica concentration of the first erupted small ash-flow layer from Rainier Mesa) to 75.5% (the highest silica content of the ash-flow layers at the base of the Pahute Mesa section). Basal layers of section two range in silica from only 74 to 75.5%. This indicates that only the upper portion

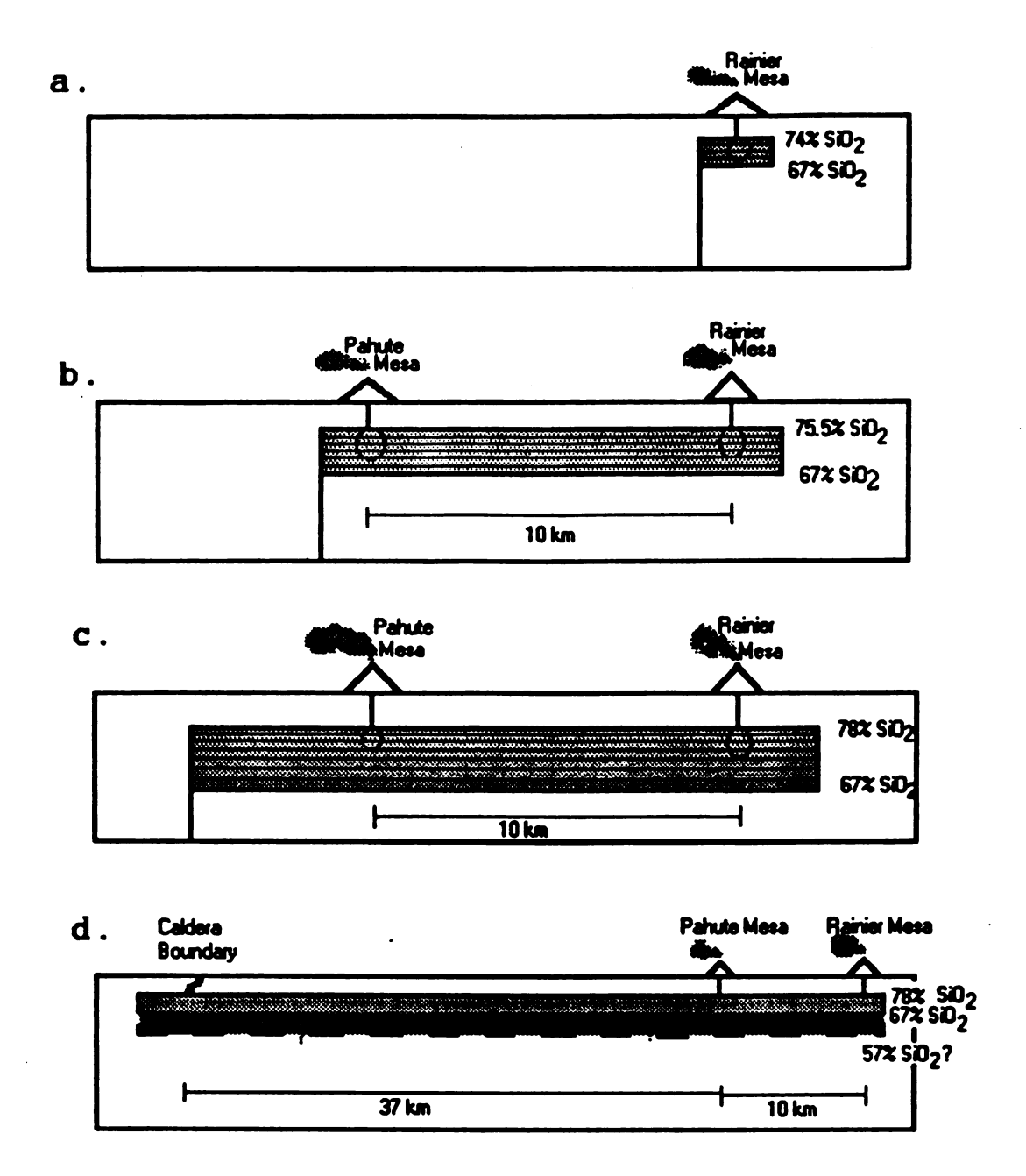


Figure 13. Schematic diagram depicting the interpreted emplacement of the Rainier Mesa magma body. Possible chemical configuration and location of Rainier Mesa magma body: a). after initial emplacement beneath the Rainier Mesa location; b). during the first eruptions at the Pahute Mesa location; c). during eruption of the uppermost small ash-flow layers in the tephra-fall sequence; d). and immediately prior to the caldera-forming eruption of the Rainier Mesa ash-flow sheet.

of the zoned magma body erupting these layers was being tapped. This pattern of eruption, growth, and recharge continued with time until the magma body ranged in silica from 67 (silica content of the first erupted layer) to 78% (the highest silica content of the last erupted small ash-flow layer in the tephra-fall sequence at each location) (Fig. 13c). By the time the Rainier Mesa ash-flow sheet was erupted, the magma body must have been at least 37 km wide if it were to underlie the tephra-fall sequence at both sample locations and extended to the furthest caldera boundary (Fig. 13d). In this case the magma body would only have to be 0.75 km thick in order to produce 1200 km³ of material.

Direct evidence for a growing magma body with time is obtained from the correlation of chemical variation with thickness of each small ash-flow layer from the Rainier Mesa location. Here, ash-flow layers become thicker towards the top of the section (Fig. 7), while the within-layer variation decreases toward the top of the section (Fig. 10). This trend could occur as a result of tapping a progressively larger magma body with time. In other words, it is reasonable to assume that as the magma body grew in size, the chemical zoning would not be as intense as the smaller, initial magma body.

Regardless of whether this model for the Rainier Mesa magmatic system is correct, the evidence against the existence of a large magma body, present in its entirety throughout the

duration of eruption of the tephra-fall sequences, is solid. This interpretation has general implications for the emplacement of large-volume high-level silicic magmas. It is reasonable to consider emplacement of large-volume, high-level magmas as a step by step progression of smaller processes contributing to the overall emplacement of the large magma body.

In conclusion, the tephra-fall sequence underlying the Rainier Mesa ash-flow sheet is compositionally equivalent to it. The tephra-fall sequence has been considered the first erupted material from the uppermost fractionated portion of the 1200 km³ Rainier Mesa magma chamber. The chemical range of pumices and whole-rock samples from the tephra-fall sequence (67-78% SiO₂, for example) indicates that eruption from the most fractionated top of a 1200 km³ chemically zoned magma body was not the source of these deposits.

Small scale chemical zoning within small ash-flow layers contained in the tephra-fall sequence is characterized by less evolved compositions, upward. This trend is consistent with the eruption of a chemically zoned magma. Superimposed on the within-layer trends are opposing large-scale among-layer trends; consistent with eruption of a continuously evolving magma.

Because the volume of each small ash-flow layer is negligible compared to that of the high-silica portion of the Rainier Mesa ash-flow, eruption dynamics and time constraints

on magma chamber evolution most likely indicate that the large-volume Rainier Mesa magma body was emplaced incrementally and that each small ash-flow layer provides a window into Rainier Mesa Member's magma body development.

APPENDICIES

Appendix 1. Major and trace element analyses of whole rock samples from small ash-flow layers and from individual pumice fragments in the tephra-fall sequence beneath the Rainier Mesa ash-flow sheet.

		Small ash-flow lay	ers from the Raini	er Mesa section		
Sample	R17A;24	R17A;13	R17A;12	R17A;11	R17A;7	R17A;2
		Weight	Percent Oxide (w	1. %)		
SiO ₂	70.82	66.58	65.10	66.27	68.03	68.56
TiO ₂	0.21	0.52	0.56	0.46	0.37	0.34
Al ₂ O ₃	13.75	15.34	16.19	15.04	15.08	15.18
FeO	1.14	3.08	2.87	2.52	2.00	1.96
MnO	0.11	0.12	0.13	0.11	0.08	0.08
MgO	0.35	1.07	0.95	1.03	0.81	0.74
CaO	0.47	1.63	1.36	1.56	1.84	1.65
Na ₂ O	3.33	3.40	3.41	3.57	3.51	3.52
K ₂ O	5.36	4.23	4.12	4.28	4.88	4.95
P ₂ O ₅	0.01	0.03	0.04	0.03	0.03	0.03
Total	95.55	96.00	94.73	94.87	96.63	97.01
		X-ray	Fluorescence (pp	m)		
Cr	0.00	0.00	0.00	0.00	0.00	0.00
Ni	0.00	1.00	1.43	6.83	0.00	4.78
Cu	0.00	0.00	0.00	0.00	0.00	0.00
Zn	66.42	79.61	72.60	73.59	44.23	48.37
Rb	165.66	136.16	122.75	146.71	145.33	153.02
Sr	72.69	292.72	313.53	280.41	337.39	303.50
Y	38.04	36.58	38.99	41.98	32.37	28.58
Zr	239.64	359.20	545.62	339.97	244.87	245.04
Nb	24.45	20.62	20.16	17.45	13.03	22.10
La	66.12	73.39	110.98	67.49	73.03	71.73
Ba	281	838	1980	791	939	952
			INAA (ppm)			
Sm		32.10			33.43	
La		181.03			181.79	
Eu		21.16			25.07	
Hf		10.19			7.97	
Ce		136.84			137.42	
Yb		15.00			14.60	
Lu		16.76			16.18	
Th		23.64			22.97	
Cr		21.25			16.30	
Ba		970			1103	
Cs		5.57			4.12	
Sc		8.17			6.17	
Ta		1.40			1.14	
Тъ		23.44			25.53	

Small ash-flow layers the from Rainier Mesa section								
Sample	R17A;1	R17B;11	R17B;7	R17B;5.5	R17B;4.5	R17B;3.		
		Weigh	nt Percent Oxide (w	l. %)				
SiO ₂	66.80	68.56	67.62	69.22	69.59	69.08		
TiO ₂	0.36	0.39	0.43	0.34	0.31	0.36		
Al ₂ O ₃	15.55	15.20	15.07	14.67	14.69	14.61		
FeO	2.16	1.66	1.80	1.49	1.55	1.93		
MnO	0.08	0.11	0.11	0.10	0.10	0.09		
MgO	0.74	0.44	0.43	0.47	0.50	0.42		
CaO	1.93	1.03	0.94	0.78	0.79	1.04		
Na ₂ O	3.66	3.41	3.42	3.16	3.12	3.21		
K ₂ O	4.85	6.02	5.85	5.71	5.49	5.33		
P ₂ O ₅	0.03	0.05	0.05	0.02	0.03	0.04		
Total	96.16	96.87	95.72	95.96	96.17	96.11		
		X-m	ry Fluorescence (pp	m)				
Cr	1.31	2.63	0.00	0.00	4.85	0.00		
Ni	6.81	16.82	0.00	4.42	7.35	0.00		
Cu	0.54	0.00	4.06	0.00	0.00	3.10		
2n	47.92	62.37	69.4 7	54.25	67.52	73.57		
Rb	133.89	158.98	167.43	177.46	177.33	164.18		
Sr	380.09	121.18	121.22	96.19	101.26	143.94		
Y	32.27	31.21	36.10	34.18	32.31	37.50		
Zr	246.13	359.31	394.55	323.96	269.87	295.59		
Nb	6.60	12.36	7.24	24.29	23.44	18.07		
La	94.42	68.15	90.17	92.57	53.74	60.61		
Ba	1188	824	857	677	444	427		
			INAA (ppm)					
Sm	29.34		33.20		29.50			
La	185.88		377.45		186.73			
Eu	29.86		40.14		26.38			
Hf	7.75		10.70		7.58			
Ce	138.70		256.89		170.28			
Υъ	14.60		14.00		13.10			
Lu	15.29		15.00		11.18			
Th	21.74		21.33	•	17.94			
Cr	15.89		3.43		8.42			
Ba	1456		1082		746			
Cs	4.06		2.90		3.28			
Sc	6.61		4.93		3.50			
Ta	1.10		0.92		1.14			
Тъ	21.91		27.66		25.32			

Small ash-flow layers from the Rainier Mesa section							
Sample	R17B;2	R17B;0	R16;2	R15;0	R14;7	R14;5.	
		Weight	Percent Oxide (wt.				
SiO ₂	67.06	64.41	72.54	69.14	69.28	68.72	
TiO ₂	0.43	0.57	0.23	0.28	0.38	0.37	
Al ₂ O ₃	14.97	16.20	13.07	13.55	13.79	13.92	
FeO	2.10	3.11	1.21	1.49	2.06	1.96	
MnO	0.10	0.09	0.07	0.07	0.08	0.09	
MgO	0.61	1.01	0.32	0.50	0.75	0.68	
CaO	1.30	2.42	0.72	0.85	1.34	1.34	
Na ₂ O	3.37	3.38	3.10	3.35	3.37	3.52	
K ₂ O	5.33	4.70	5.47	5.20	4.82	4.90	
P ₂ O ₅	0.05	0.12	0.01	0.01	0.03	0.04	
Total	95.32	96.01	96.74	94.44	95.90	95.54	
			Fluorescence (ppn				
Cr	0.00	11.87	. 0.00	0.00	3.34	0.00	
Ni	0.00	1.72	0.00	0.00	0.00	0.00	
Cu	0.00	16.04	0.00	0.00	21.44	7.31	
Zn	72.27	65.88	1247.10	47.14	139.65	85.87	
Rb	157.19	145.30	176.40	174.60	160.12	160.59	
Sr	168.38	395.08	72.90	105.89	193.83	187.47	
Y	32.99	34.19	33.88	39.51	38.09	41.06	
Zr	356.91	293.00	188.99	207.19	216.47	210.87	
Nb	17.88	16.84	25.91	22.71	22.35	20.90	
La	88.41	60.64	60.24	75.97	57.13	88.89	
Ba	530	768	255	358	454	292	
			INAA (ppm)				
Sm	33.20		31.60		31.88	32.93	
La	352.61		176.94		183.76	166.45	
Eu	33.33		15.07		20.00	19.13	
Hf	9.94		6.59		6.95	6.72	
Ce	236.98		129.16		138.34	128.55	
ΥЪ	14.65		15.10		16.15	14.90	
Lu	15.59		16.47		18.53	15.59	
Th	22.57		28.08		26.99	22.07	
Cr	5.02		5.25		13.93	7.47	
Ba	885		334		503	442	
Cs	3.57		4.75		5.47	4.36	
Sc	5.67		3.68		6.61	4.57	
Ta	1.01		1.47		1.35	1.18	
Тъ	30.85		28.30		25.74	26.38	

		Small ash-flow l	ayers from the Raini	er Mesa section		
Sample	R14;4	R14;1.5	R13;18.5	R13;9	R13;3.5	R13;0.5
		Weig	ht Percent Oxide (w	t. %)		
SiO ₂	70.09	69.27	68.55	68.94	68.83	69.60
TiO ₂	0.35	0.37	0.28	0.29	0.27	0.28
Al ₂ O ₃	14.27	14.05	15.26	15.32	14.89	14.83
FeO	1.86	2.10	1.44	1.44	1.37	1.45
MnO	0.08	0.09	0.08	0.08	0.08	0.09
MgO	0.67	0.78	0.31	0.54	0.42	0.46
CaO	1.29	1.44	1.05	0.93	0.91	0.97
Na ₂ O	3.15	3.21	3.15	3.02	3.13	3.28
K₂O	5.00	4.84	5.56	5.34	5.24	5.31
P ₂ O ₅	0.03	0.05	0.04	0.04	0.02	0.03
Total	96.79	96.20	95.72	95.94	95.16	96.30
			ray Fluorescence (pp	m)		
Cr	9.08	0.00	0.00	4.58	19.41	7.00
Ni	1.54	0.92	0.00	0.00	0.00	0.00
Cu	5.84	0.00	5.86	0.00	2.90	4.31
Zn	58.81	57.04	56.37	59.71	53.96	57.40
Rb	158.28	149.97	173.54	174.40	176.71	163.49
Sr	168. 99	207.48	148.52	123.17	111.70	126.55
Y	36.34	40.32	36.66	39.45	31.80	35.80
Zr	187. 5 6	197.36	222.36	229.57	223.96	228.03
Nb	26.55	12.18	29.22	26.26	23.61	7.41
La	61.01	70.52	53.69	85.14	55.30	58.33
Ba	69	342	327	292	6	158
-			INAA (ppm)			
Sm			37.40			30.28
La			227.30			180.61
Eu			21.74			18.99
Hf			7.36			7.30
Ce			152.06			138.20
Υъ			15.80			14.35
Lu			16.76			14.71
Th			26.73			23.04
Cr			10.57			3.60
Ba			555			486
Cs			5.60			4.38
Sc			4.24			3.04
Ta			1.63			1.19
Тъ			23.62			22.77

	Small ash-flow layers from the Rainier Mesa section							
Sample	R12;26	R12;22	R12;18	R12;15	R12;13	R12;7.5		
		Weight	Percent Oxide (wt.	%)				
SiO ₂	70.04	69.98	70.24	68.42	68.15	68.73		
TiO,	0.33	0.34	0.33	0.35	0.42	0.36		
Al ₂ O ₃	14.41	14.47	14.71	14.95	15.60	14.84		
FeO	1.66	1.82	1.70	1.88	2.29	2.06		
MnO	0.09	0.08	0.09	0.09	0.10	0.10		
MgO	0.57	0.70	0.68	0.79	1.10	0.85		
CaO	1.10	1.30	1.25	1.26	1.24	1.25		
Na ₂ O	3.28	3.32	3.37	3.49	3.40	3.34		
K ₂ O	5.08	4.81	4.92	4.78	4.47	4.64		
P ₂ O ₅	0.03	0.02	0.03	0.03	0.03	0.03		
Total	96.59	96.84	97.32	96.04	96.80	96.20		
		X-ray	Fluorescence (ppm	1)				
Cr	11.12	7.22	9.73	10.02	23.38	5.11		
Ni	0.00	0.00	0.00	0.00	20.03	4.25		
Cu	2.03	3.64	0.00	12.23	9.46	1.57		
Z n	57.52	53.90	53.65	63.48	69.07	56.68		
Rb	150.42	155.34	147.18	155.41	156.61	151.47		
Sr	146.01	173.28	166.42	175.48	1 69 .53	171.18		
Y	35.75	34.47	39.61	38.47	46.44	46.58		
Zr	223.80	214.43	217.66	233.28	271.78	210.71		
Nb	28.36	34.82	29.97	24.99	18.89	19.08		
La	44.70	57.86	63.30	66.20	64.90	14.82		
_								

INAA (ppm)

Sm	31.44
La	192.73
Eu	18.12
Hf	7.43
Ce	139.74
ΥЪ	14.35
Lo	14.71
Th	21.68
Cr	7.05
Ba	488
Cı	4.27
Sc	3.27
Ta	1.07
Тъ	21.06

Appendix 1. Continued

		Small ash-flow lay	ers from the Rainic	r Mesa section		
Sample	R12;1.75	R12;0	R3;200	R3;188	R3;156	R3;12
			Percent Oxide (wt.			
SiO ₂	67.16	68.42	77.24	74.26	73.21	73.80
TiO,	0.44	0.42	0.11	0.10	0.14	0.20
Al ₂ O ₃	15.44	15.30	12.79	12.62	12.91	12.39
FeO	2.65	2.56	0.73	0.69	0.91	1.25
MnO	0.10	0.10	0.07	0.07	0.07	0.06
MgO	0.77	0.66	0.71	0.62	0.90	0.75
CaO	1.49	1.38	0.50	0.46	0.48	0.71
Na ₂ O	3.49	3.53	2.94	2.89	2.85	2.91
K₂O	4.51	4.71	4.89	4.71	4.73	4.13
P ₂ O ₅	0.03	0.03	0.01	0.01	0.01	0.02
Total	96.08	97.11	96.29	96.43	96.78	96.22
			Fluorescence (ppm			
Cr	1.18	0.00	0.00	0.00	0.00	0.00
Ni	4.96	7.02	0.00	0.00	0.00	0.00
Cu	0.00	0.00	0.00	0.00	0.00	0.00
Zn	91.18	77.43	39.15	30.72	32.33	43.00
Rb	133.95	132.94	238.96	224.60	212.13	198.82
Sr	201.81	177.25	17.71	22.37	51.18	83.20
Y	53.60	56.90	23.77	21.13	21.97	25.03
Zr	257.91	243.50	88.81	78.99	102.05	115.25
NЪ	22.78	17.06	28.11	26.63	28.79	27.50
<u>La</u>	43.51	35.44	15.51	31.46	31.28	34.51
Ba	136	178	34	117	186	219
			INAA (ppm)			
Sm	31.88	35.30	30.99		30.83	30.33
La	252.24	196.33	78.39		80.18	56.42
Eu	24.20	25.07	1.16		2.75	4.35
Hf	7.84	7.25	3.67		4.01	3.88
Ce	156.67	140.81	59.77		72.58	58.20
Υъ	18.80	16.25	13.90		13.80	12.60
Lu	21.76	14.12	14.41		15.29	10.59
Th	26.87	17.67	24.62		27.45	16.20
Cr	17. 99	14.27	4.64		6.85	10.09
Ba	501	488	137		213	247
Cı	5.58	3.85	5.80		6.07	6.63
Sc	6.26	3.93	4.13		4.64	3.34
Ta	1.66	1.24	2.06		1.87	1.44
Тъ	23.64	52.34	11.43		9.15	13.19

Appendix 1. Continued

Small ash-flow layers from the Rainier Mesa section						
Sample	R3;58	R3;3	R2;30	R1;129	R1;117	R1;94
		Weight	Percent Oxide (wt. 9	%)		
SiO ₂	73.76	73.15	74.39	75.03	74.88	74.57
TiO ₂	0.18	0.21	0.10	0.11	0.11	0.12
Al ₂ O ₃	12.22	12.40	12.15	11.63	12.04	12.32
FeO	1.11	1.31	0.68	0.68	0.71	0.83
MnO	0.07	0.07	0.06	0.07	0.06	0.06
MgO	0.42	0.65	0.19	0.14	0.26	0.23
CaO	0.65	0.67	0.42	0.47	0.45	0.50
Na ₂ O	3.03	3.04	3.28	3.10	3.21	3.20
K ₂ O	4.48	4.24	4.68	4.66	4.64	4.67
P,O,	0.02	0.02	0.01	0.01	0.01	0.01
Total	95.94	95.76	95.96	95.90	96.37	96.51
			Fluorescence (ppm)	-		
Cr	0.00	0.00	0.00	0.00	0.00	0.00
Ni	0.00	6.73	1.29	0.00	6.14	29.40
Cu	0.00	0.00	0.00	0.00	0.00	1.66
Zn	45.90	52.17	20.59	22.39	26.75	74.71
Rb	226.11	213.74	246.52	235.40	224.86	237.02
Sr	68.72	76.33	14. 69	15.99	15.15	30.42
Y	30.81	32.93	28.32	32.26	29.64	30.18
Zr	107.49	133.08	80.72	80.61	78.78	91.76
Nb	26.32	24.19	23.55	21.64	22.52	20.94
La	18.59	51.76	9.69	40.53	51.74	40.70
Ba	268	196	0	81	83	95
			INAA (ppm)			
Sm	28.90		29.61			
La	78.52		53.85			
Eu	3.91		0.58			
Hf	4.02		3.19			
Ce	68.76		50.32			
Yъ	14.75		14.30			
Lo	14.41		14.12			
Th	23.75		19.26			
Cr	8.27		3.45			
Be	231		96			
Cı	8.29		8.85			
Sc	5.16		3.43			
Ta	2.11		1.96			
Тъ	15.53		15.74			

Appendix 1. Continued

	Small ash-flow layers from the Rainier Mesa section							
Sample	R1;78	R1;54	R1;31	R1;18	R1;14	R1;		
			t Percent Oxide (wt.					
SiO ₂	73.84	73.68	75.16	74.75	75.92	75.03		
TiO ₂	0.13	0.14	0.12	0.11	0.16	0.17		
Al ₂ O ₃	12.32	12.32	11.89	12.38	11.95	12.15		
FeO	0.78	0.96	0.90	0.71	1.06	1.22		
MnO	0.06	0.07	0.06	0.07	0.04	0.05		
MgO	0.28	0.31	0.23	0.69	0.35	0.42		
CaO	0.51	0.58	0.54	0.48	0.62	0.63		
Na ₂ O	3.27	3.40	3.08	2.85	2.93	3.06		
K ₂ O	4.61	4.51	4.48	4.73	4.42	4.36		
P,O,	0.01	0.01	0.01	0.01	0.02	0.02		
Total	95.81	95.98	96.47	96.78	97.47	97.11		
		X-ra	y Fluorescence (ppm	1)				
Cr	0.00	0.00	0.00	16.05	0.00	0.00		
Ni	6.80	8.40	8.58	0.00	5.73	6.99		
Cu	0.00	0.00	0.21	0.00	0.00	12.96		
2n	283.55	1134.93	26.36	35.77	22.97	692.77		
Rb	233.02	224.24	211.82	185.87	176.76	179.59		
Sr	31.60	46.63	36.49	85.05	68.69	85.59		
Y	28.49	31.27	22.56	30.82	20.05	21.03		
Zr	86.81	82.40	78.57	100.65	86.60	99.38		
Nb	19.46	18.55	20.03	15.11	16.96	15.06		
La	73.84	45.20	35.21	8.31	47.42	42.92		
Ba	0	34	20	38	119	192		
			INAA (ppm)					
Sm	•	31.82		26.91	27.02			
La		59.18		50.30	67.12			
Ea		2.03		4.06	2.75			
Hf		3.77		3.53	3.50			
Ce		58.43		51.92	54.11			
ΥЪ		14.90		12.20	12.40			
ما		16.76		8.82	11.47			
Th		23.03		12.23	19.18			
Cr		8.03		9.07	7.94			
Ba		127		179	229			
Cs		11.29		8.15	11.64			
Sc		5.40		1.99	4.42			
Ta		2.32		1.34	1.74			
Тъ		12.77		15.96	15.77			

Small ash-flow layers from the Pahute Mesa section						
Sample	P19;1	P19;9	P19;18	P19;25	P23;0	P23;4
			ht Percent Oxide (w			
SiO ₂	72.06	71.34	70.38	72.10	70.42	70.42
TiO ₂	0.16	0.22	0.18	0.19	0.19	0.18
Al ₂ O ₃	12.91	13.17	13.19	13.48	13.57	13.66
FeO	1.29	1.79	1.43	1.64	1.55	1.57
MnO	0.09	0.09	0.08	0.09	0.10	0.10
MgO	0.20	0.02	0.09	0.18	0.39	0.43
CaO	0.86	0.97	1.04	1.05	0.72	0.73
Na ₂ O	3.33	3.22	3.54	3.38	3.52	3.31
K₂O	4.53	4.45	4.41	4.47	4.93	5.04
P ₂ O ₅	0.02	0.01	0.01	0.02	0.02	0.02
Total	95.45	95.28	94.35	96.60	95.41	95.46
			ray Fluorescence (pp	m)		
Cr	2.17	1.38	3.83	0.00	3.15	0.00
Ni	0.00	0.00	0.00	0.00	0.00	0.00
Cu	0.00	2.44	0.00	16.14	5.92	11.28
Zn	57.01	59.97	55.95	63.07	71.08	64.01
Rb	163.11	158.58	155.40	151.03	151.18	152.54
Sr	152.48	170.29	190.99	191.49	95.18	92.20
Y	32.98	32.74	35.44	30.72	34.81	41.12
Zr	167.07	207.40	192.74	200.98	212.13	216.76
Nb	16.19	3.70	7.35	10. 69	15.91	16.64
La	78.04	164.99	139.77	126.26	134.68	179.09
Ba	159	190	283	241	69	57
			INAA (ppm)			
Sm			-			5.78
La						99.46
Eu						0.51
Hf						7.06
Ce						179.19
Yb						2.89
Lu						0.54
Th						24.58
Cr						3.28
Ba						381
Cs						3.57
Sc						2.50
Ta						1.36
Тъ						0.99

Appendix 1. Continued.

Small ash-flow layers from the Pahute Mesa section						
Sample	P23;9	P24A;2	P24A;7	P24A;15	P24;1	P24;
			Percent Oxide (pp			
SiO ₂	70.52	72.71	74.47	74.68	72.43	72.63
TiO ₂	0.16	0.22	0.09	0.10	0.13	0.11
Al ₂ O ₃	13.49	12.31	11.96	11.93	12.42	12.32
FeO	1.44	1.91	1.07	0.98	1.33	1.12
MnO	0.09	0.08	0.07	0.07	0.08	0.08
MgO	0.45	0.47	0.19	0.15	0.13	0.09
CaO	0.69	0.98	0.47	0.49	0.62	0.54
Na ₂ O	3.29	2.97	3.12	3.02	3.07	3.07
K₂O	4.97	4.64	4.89	4.95	4.93	4.98
P ₂ O ₃	0.01	0.02	0.01	0.01	0.01	0.01
Total	95.11	96.31	96.34	96.38	95.15	94.95
			Fluorescence (ppm			
Cr	0.00	18.63	4.50	0.00	0.00	2.37
Ni	0.00	30.87	0.00	0.00	0.00	0.00
Cu	0.00	8.76	9.39	0.00	22.60	0.00
Zn	61.63	63.94	57.11	56.85	62.58	59.31
Rь	152.42	160.23	167. 79	172.14	173.24	171.89
Sr	86.47	86.02	23.43	30.85	66.72	48.12
Y	38.94	42.22	41.52	43.70	39.51	38.84
Z r	189.86	133.09	122.06	130.91	154.61	134.24
Nb	21.65	26.85	28.05	28.21	27.22	18.60
La	108.21	101.74	64.75	102.61	82.33	71.42
Ba	146	18	0	45	70	0
			INAA (ppm)			
Sm	5.64	5.72		· · · · · · · · · · · · · · · · · · ·		5.79
La	83.00	38.26				33.74
Eu	0.42	0.17				0.12
Hf	6.54	6.21				5.51
Ce	153.55	85.57				73.93
Υъ	2.84	3.11				3.15
Lu	0.52	0.54				0.56
Th	8.00	22.61				22.19
Cr	3.33	3.50				3.28
Ba	286	224				169
Cs	3.33	4.09				3.67
Sc	1.92	2.04				1.43
Ta	1.35	1.54				1.48
Тъ	1.10	1.00				1.10

Small ash-flow layers from the Pahute Mesa section P0;3 Sample P24;27 P0;0.5 P0;6 P1;0.5 P1;3 Weight Percent Oxide (wt. %) 74.16 SiO2 74.30 69.79 71.31 73.94 73.66 0.13 0.09 0.10 TiO2 0.08 0.16 0.10 12.14 13.30 12.92 12.28 12.07 Al₂O₃ 14.18 FeO 1.07 1.43 1.09 0.89 0.89 0.87 0.06 0.06 0.06 MnO 0.07 0.07 0.06 0.12 0.25 0.17 0.00 0.08 0.07 MqO CaO 0.43 0.70 0.62 0.63 0.71 0.56 Na₂O 2.95 3.28 2.63 2.95 2.97 3.02 K_2O 5.11 4.38 4.70 5.01 4.98 4.97 P_2O_5 0.01 0.01 0.01 0.01 0.01 0.01 Total 96.25 94.49 95.83 95.91 95.91 94.26 X-ray Fluorescence (ppm) Cr 8.16 0.62 0.00 0.00 0.65 2.18 Νi 0.00 12.09 6.40 3.00 6.30 5.65 0.00 Cu 1.67 1.35 0.00 0.00 0.00 Zn 62.03 37.01 27.33 23.85 29.45 26.45 Rb 171.54 166.34 171.77 175.29 179.09 169.29 Sr 19.39 71.38 63.12 22.60 43.79 43.19 Y 43.29 26.93 27.26 23.86 28.55 28.28 130.93 118.98 102.01 86.96 98.79 94.67 Zr Nb 24.80 15.20 17.27 20.03 18.30 18.03 La 60.85 60.16 52.45 71.19 63.85 48.59 Ba 0 12 54 179 76 192 INAA (ppm) 5.68 Sm 5.34 5.80 La 29.54 24.90 34.46 0.22 Eu 0.40 0.31 Ηf 4.48 3.73 4.08 Ce 66.95 60.87 70.36 Yb 2.88 2.38 2.76 0.49 0.31 0.48 Lu Th 29.24 19.05 27.62 Cr 9.41 3.28 6.17 Ba 176 118 137 Cs 5.73 4.74 5.55 Sc 4.79 2.58 3.44 1.38 Ta 1.38 1.30 0.79 Tb 0.91 0.66

Appendix 1. Continued.

		Small ash-flow lay	ers from the Pahute	Mesa section		
Sample	P1;6	P1;10	P1;20	P1;25	P2;2	. P2;0
		Wei	cht Percent (wt. %)			
SiO ₂	72.90	73.92	74.43	73.72	73.85	75.78
TiO ₂	0.16	0.12	0.09	0.09	0.08	0.07
Al ₂ O ₃	12.95	12.59	12.10	12.12	12.02	12.24
FeO	1.29	1.11	0.89	0.78	0.90	0.67
MnO	0.07	0.06	0.06	0.06	0.06	0.06
MgO	0.22	0.15	0.05	0.05	0.01	0.00
CaO	0.74	0.72	0.57	0.58	0.58	0.55
Na ₂ O	2.81	2.85	2.78	2.83	2.98	2.97
K ₂ O	4.84	4.90	5.04	5.06	4.96	5.01
P ₂ O ₅	0.02	0.01	0.00	0.01	0.00	0.00
Total	96.00	96.43	96.01	95.30	95.44	97.35
		X-ray	Fluorescence (ppm)			
Cr	0.00	8.93	0.00	7.52	0.00	0.00
Ni	6.14	31.47	1.55	9.32	2.67	0.00
Cu	0.00	0.00	0.00	0.00	2.42	0.00
Zn	30.69	27.23	28.64	23.56	29.70	24.13
Rb	166.24	167.24	180.75	182.72	185.14	186.89
Sr	85 .61	64.45	37.08	37.88	28.53	14.51
Y	32.80	29.18	21.61	19.23	21.99	28.14
Zr	114.47	93.56	99 .78	95.02	84.59	77.65
Nb	15.38	16.68	23.13	19.33	21.80	20.91
La	95.29	82.87	69.92	79.44	62.43	37.32
Ba	154	167	0	75	0	69
			INAA (ppm)			
Sm		5.92		5.68	5.72	
La		113.09		24.90	24.21	
Eu		2.30		0.22	0.19	
Hf		9.16		3.73	3.92	
Ce		183.26		60.87	60.73	
Υъ		2.72		2.38	2.81	
Lu		0.41		0.31	0.48	
Th		19.12		19.05	29.48	
Cr		9.59		5.51	4.49	
Ba		798		128	115	
Cı		3.53		4.06	5.62	
Sc		5.04		1.97	3.63	
Ta		1.07		1.16	1.55	
Тъ		1.00		0.71	0.73	

	Small ash-flow layers from the Pahute Mesa section							
Sample	P2;8	P3;0	P3;6	P3;12				
	Weight Percent Oxide (wt. %)							
SiO ₂	74.08	73.43	73.58	72.55				
TiO ₂	0.07	0.11	0.08	0.08				
Al ₂ O ₃	11.95	12.29	11.98	12.25				
FeO	0.76	1.00	0.79	0.88				
MnO	0.06	0.07	0.06	0.06				
MgO	0.02	0.13	0.12	0.32				
CaO	0.55	0.65	0.57	0.56				
Na2O	2.85	2.73	2.82	2.70				
K₂O	4.99	5.14	5.17	5.17				
P ₂ O ₅	0.01	0.02	0.02	0.01				
Total	95.34	95.57	95.19	94.58				
	X-ray Fluorescence (ppm)							
Cr	0.00	25.68	0.00	2.24				
Ni	0.00	54.42	0.00	0.00				
Cu	0.00	0.00	0.00	7.43				
Zn	35.10	35.86	35.57	33.07				
Rb	190.70	190.88	183.15	190.09				
Sr	24.94	55.75	37.40	44.10				
Y	31.96	30.84	30.61	30.52				
Zr	77.91	92.60	87.39	89.05				
Nb	12.06	12.44	13.99	15.48				
La	70.86	86.70	69.66	83.91				
Ba	0	18	0	0				
	INAA (ppm)							
Sm	6.28	5.87		5.68				
La	0.00	30.96		27.60				
Eu	0.16	0.26		0.24				
Hf	3.94	4.28		3.80				
Ce	61.01	68.68		62.49				
Υь	2.79	2.72		2.48				
Lu	0.50	0.51		0.42				
Th	30.50	30.85		24.49				
Cr	4.49	5.43		3.28				
Ba	71	157		139				
Cs	5.49	6.28		4.14				
Sc	3.46	4.10		2.43				
Ta	1.58	1.46		1.38				
Тъ	0.67	0.58		0.96				

Appendix 1. Continued.

Tehpra-fall sequence (individual pumice fragments)

Sample	M7PRA	MPRG	M13C	M14A	M14B	M20B				
Weight Percent Oxide (wt. %)										
SiO ₂	77.27	76.80	75.43	75.83	75.37	76.25				
TiO ₂	0.08	0.07	0.14	0.13	0.14	0.08				
Al ₂ O ₃	12.56	12.49	14.06	13.23	13.70	13.00				
FeO	0.83	1.04	1.25	1.36	1.24	1.00				
MnO	0.06	0.06	0.13	0.06	0.07	0.08				
MgO	0.25	0.16	0.49	0.25	0.37	0.22				
CaO	0.61	0.77	0.62	0.75	0.88	0.50				
Na ₂ O	2.92	3.16	2.88	3.11	3.13	3.71				
K ₂ O	5.40	5.45	4.99	5.27	5.08	5.14				
P ₂ O ₅	0.01	0.01	0.01	0.01	0.01	0.01				
Total	97.14	96.51	95.73	95.00	94.24	95.24				
X-ray Fluorescence (ppm)										
Cr	6.50	6.00	2.60	0.00	2.40	6.90				
Ni	0.00	5.80	0.20	10.80	0.00	8.00				
Cu	60.20	61.40	60.30	65.00	60.00	63.30				
Zn	33.30	27.60	45.40	66.20	45.60	55.50				
Rb	198.30	203.10	185.30	195.30	193.60	192.20				
Sr	33.10	53.10	53.00	97.80	131.30	53.00				
Y	35.60	34.40	48.40	39.30	38.50	40.10				
Zr	81.30	85.60	114.60	132.00	130.00	105.00				
Nb	30.70	12.80	26.80	20.70	29.20	33.00				
La	21.30	20.00	18.70	24.70	22.20	35.10				
Ba	176	219	422	377	318	237				

[•] sample names beginning with both the letters M and P are from the Pahute Mesa section. Sample names beginning with the letter R are from the Rainier Mesa section.

Appendix 1. Continued.

Tephra-fall sequence (individual pumice fragments)

Sample	M20F	M20G	M21,1A	M21,1D	M21,2D	M21,2E
		Weig	ht Percent (wt. %)			
SiO ₂	76.72	76.57	76.22	71.00	75.64	76.13
TiO ₂	0.08	0.09	0.10	0.42	0.10	0.10
Al ₂ O ₃	12.70	12.84	13.02	15.08	13.34	13.39
FeO	0.98	0.77	1.24	2.61	1.13	0.84
MnO	0.08	0.08	0.09	0.09	0.08	0.08
MgO	0.01	0.19	0.09	0.56	0.05	0.05
CaO	0.53	0.50	0.59	1.81	0.50	0.49
Na ₂ O	3.75	3.65	3.43	3.84	3.77	3.51
K₂O	5.13	5.29	5.20	4.47	5.38	5.39
P ₂ O ₅	0.01	0.01	0.01	0.12	0.01	0.01
Total	95.96	95.32	95.49	95.23	94.18	95.61
		X-ray	Fluorescence (ppm)	1		
Cr	0.00	7.30	4.30	6.90	3.80	0.00
Ni	3.70	0.00	9.90	9.00	0.00	0.00
Cu	60.50	57.00	61.60	64.00	59.60	58.60
Zn	52.80	48.60	58.50	79.30	72.00	52.70
Rb	190.70	185.40	187.30	147.40	160.50	164.60
Sr	49.00	46.80	67.60	249.70	28.20	27.10
Y	40.40	40.60	38.30	37.90	39.90	38.10
Zr	92.80	95.60	116.30	279.80	150.40	149.30
Nb	24.00	27.90	32.60	16.50	23.20	18.60
La	59.90	37.70	43.40	82.50	37.40	54.20
Ba	248	284	370	640	168	131

Appendix 1. Continued.

Tephra-fall sequence (individual pumice fragments)

			•			
Sample	M21,3E	M21,3F	M21,4D	M21,6J	M21,6Q	M22,1D
		We	eight Percent (wt. %)		
SiO ₂	77.09	76.71	67.53	74.07	72.45	75.65
TiO ₂	0.08	0.08	0.39	0.20	0.22	0.11
Al ₂ O ₃	12.92	12.74	17.00	14.25	14.39	13.73
FeO	0.83	1.16	2.68	1.46	1.33	1.02
MnO	0.09	0.08	0.15	0.08	0.09	0.08
MgO	0.53	0.10	0.61	0.19	0.25	0.04
CaO	0.48	0.52	1.79	0.80	0.92	0.55
Na ₂ O	3.16	3.53	4.98	3.86	5.36	3.46
K₂O	4.80	5.05	4.86	5.06	4.97	5.35
P ₂ O ₅	0.01	0.01	0.01	0.02	0.03	0.01
Total	95.14	95.58	96.00	94.79	92.70	95.06
		Х-га	y Fluorescence (ppn	n)		
Cr	8.30	2.60	6.50	0.00	8.80	16.10
Ni	0.00	20.30	0.00	0.80	0.00	0.00
Cu	59.40	59.80	59.00	61.60	57.40	56.30
Zn	68.20	56.00	103.90	52.60	44.90	52.00
Rb	166.30	180.00	164.20	157.50	160.70	160.90
Sr	47.30	50.90	307.80	97.80	130.70	43.00
Y	41.90	41.10	42.70	34.70	35.00	46.60
Zr	125.50	99.10	505.70	219.20	249.40	185.40
Nb	17.50	23.90	16.60	24.60	23.20	34.20
La	43.20	44.20	130.40	92.40	58.70	55.20
Ba	231	232	938	541	683	241

Appendix 1. Continued.

Tephra-fall sequence (individual pumice fragments)

Sample	M22,1E	M22,4A	M22,4B	M23,6A	M23,6B	M24,2A
		We	eight Percent (wt. %	o)		
SiO ₂	75.08	75.89	75.35	77.21	77.41	76.26
TiO ₂	0.11	0.09	0.13	0.07	0.07	0.08
Al ₂ O ₃	13.78	13.26	13.68	12.97	12.45	12.74
FeO	1.50	1.07	1.05	0.74	1.00	1.25
MnO	0.08	80.0	0.08	0.07	0.07	0.07
MgO	0.07	0.06	0.04	0.09	0.01	0.01
CaO	0.53	0.50	0.59	0.46	0.44	0.49
Na ₂ O	3.51	3.73	3.55	3.00	2.76	3.57
K,O	5.32	5.31	5.51	5.37	5.77	5.51
P ₂ O ₅	0.01	0.01	0.02	0.01	0.01	0.01
Total	94.31	94.80	95.29	95.07	95.62	95.39
		Х-га	y Fluorescence (pp	m)		
Cr	14.80	14.20	15.60	22.60	14.50	20.50
Ni	4.90	0.00	0.00	0.00	2.40	0.90
Cu	62.70	58.90	58.00	56.30	58.90	61.00
Zn	53.60	59.70	52.40	58.80	52.70	57.80
Rb	170.40	172.50	163.20	208.60	200.90	183.20
Sr	41.60	30.80	45.70	32.30	23.00	35.30
Y	43.60	41.70	43.30	43.40	46.10	43.80
Zr	179.10	159.00	188.00	124.60	114.80	138.60
Nb	39.80	36.20	36.90	14.20	31.90	28.10
La	89.10	32.80	62.90	20.30	34.30	55.50
Ba	287	271	210	180	100	20

Appendix 1. Continued.

Tephra-fall sequence (individual pumice fragments)

Sample	R7E	R7F	R8A	RIIA	R11F	R12F
		Weigh	t Percent Oxide (w	L %)		
SiO ₂	69.99	75.15	77.84	75.68	75.88	73.51
TiO ₂	0.34	0.20	0.19	0.16	0.16	0.26
Al ₂ O ₃	16.31	13.55	12.30	13.57	13.28	14.46
FeO	1.44	1.13	0.91	0.89	0.79	1.37
MnO	0.14	0.09	0.08	0.12	0.12	0.08
MgO	2.73	0.70	0.65	. 0.31	0.16	0.55
CaO	1.33	0.54	0.44	0.30	0.30	0.82
Na ₂ O	3.79	3.32	2.81	3.13	3.48	3.16
K ₂ O	3.49	5.30	4.76	5.85	5.83	5.78
P ₂ O ₅	0.43	0.01	0.01	0.01	0.01	0.01
Total	94.44	95.54	95.13	94.68	95.27	95.70
		X-ra	y Fluorescence (pp	m)		
Cr	23.50	18.10	17.10	0.00	0.30	0.00
Ni	0.00	0.00	0.00	0.00	0.00	0.00
Cu	59.70	58.10	56.90	5 7.20	57.00	58.10
Zn	76.00	61.60	51.50	63.50	63.90	50.80
Rb	126.70	204.00	184.00	191.80	187.30	207.80
Sr	131.70	61.00	38.40	24.60	21.50	102.00
Y	55.40	35.50	39.80	48.90	44.30	48.10
Zr	292.40	195.40	150.90	204.60	213.10	222.50
Nb	18.00	21.80	27.40	30.30	33.90	30.00
La	91.50	40.50	34.90	16.30	0.00	29.30
Ba	1106	386	159	139	83	437

Appendix 1. Continued.

Tephra-fall sequence (individual pumice fragments)

Sample	R14B	R15A	R16A	R17G	R17H	PMR-SURGE-E
			eight Percent Oxide			
SiO ₂	73.81	74.67	73.87	72.49	75.84	76.50
TiO ₂	0.28	0.23	0.25	0.27	0.17	0.08
Al ₂ O ₃	14.44	13.86	14.48	14.87	13.08	13.14
FeO	1.24	1.04	1.26	1.28	1.00	0.76
MnO	0.09	0.08	0.09	0.13	0.11	0.06
MgO	0.48	0.31	0.37	0.39	0.13	0.00
CaO	0.75	0.65	0.68	0.66	0.32	0.73
Na ₂ O	3.02	3.06	2.97	3.96	3.58	3.19
K ₂ O	5.86	6.07	5.99	5.92	5.75	5.52
P ₂ O ₅	0.02	0.02	0.03	0.03	0.01	0.01
Total	95.13	94.88	96.38	95.01	95.70	95.83
		2	(-ray Fluorescence	(ppm)		
Cr	0.00	0.00	2.10	0.00	2.60	0.00
Ni	0.00	0.00	0.00	0.00	0.00	0.00
Cu	58.10	57.40	57.90	56.40	57.20	58.00
Zn	44.40	55.50	42.00	64.90	74.10	24.20
Rb	192.00	203.20	192.30	167.20	187.60	222.60
Sr	79.80	63.00	60.80	74.80	25.40	36.10
Y	41.50	43.50	47.70	55.00	47.10	55.40
Zr	209.20	193.80	187.20	318.90	202.50	85.80
Nъ	37.80	38.50	34.00	38.00	39.00	41.50
La	29.70	19.30	31.20	12.50	35.10	0.80
Ba	345	190	205	282	116	124

Appendix 1. Continued

Tephra-fall sequence (individual pumice fragments)

Sample	PMR-SURGE-F	PIA	P1B	P2.1A	P2.1B	P2.3A
		Weight	Percent Oxide (wt.	. %)		
SiO ₂	75.87	76.55	77.68	77.31	77.45	76.97
TiO ₂	0.10	0.08	0.08	0.08	0.08	0.08
Al ₂ O ₃	13.55	13.08	12.55	12.92	12.83	13.01
FeO	1.16	1.11	0.62	0.75	0.99	0.85
MnO	0.06	0.05	0.05	0.06	0.05	0.06
MgO	0.11	0.02	0.00	0.00	0.00	0.00
CaO	0.64	0.56	0.56	0.56	0.57	0.57
Na ₂ O	3.22	2.87	3.00	2.54	2.59	2.95
K₂O	5.25	5.66	5.45	5.76	5.43	5.50
P ₂ O ₅	0.01	0.01	0.01	0.01	0.01	0.01
Total	96.29	95.20	95.65	95.69	96.31	95.04
		X-ray	Fluorescence (ppn	n)		
Cr	0.00	0.00	1.30	7.00	3.90	0.00
Ni	5.20	0.80	0.00	0.00	0.00	0.00
Cu	60.20	62.70	58.00	56.00	56.90	59.20
Zn	53.40	52.70	31.20	29.60	34.10	30.40
Rb	203.40	214.80	202.90	218.90	203.50	204.20
Sr	32.60	29.50	29.50	26.70	25.30	32.00
Y	31.70	28.40	27.90	25.20	25.10	27.50
Zr	99.30	91.90	86.70	87.30	83.20	88.50
Nb	22.90	21.70	27.20	27.00	22.30	15.10
La	41.20	38.20	22.80	30.20	40.70	41.70
Ba	165	146	73	87	79	216

Appendix 1. Continued.

Tephra-fall sequence (individual pumice fragments)

Sample	P2.3B	P3.1A	P3.1B	P3.1G	P3.2A	P3.2B			
Weight Percent Oxide (wt. %)									
SiO ₂	76.68	77.43	77.25	77.46	77.10	76.48			
TiO ₂	0.08	0.07	0.07	0.07	0.08	0.08			
Al ₂ O ₃	13.08	12.44	12.51	12.55	12.68	13.14			
FeO	1.08	0.58	0.92	0.69	0.93	1.05			
MnO	0.06	0.06	0.06	0.06	0.06	0.06			
MgO	0.00	0.00	0.00	0.00	0.00	0.03			
CaO	0.55	0.56	0.57	0.56	0.58	0.56			
Na ₂ O	2.91	3.17	3.35	2.86	3.21	3.21			
K ₂ O	5.54	5.67	5.25	5.73	5.34	5.37			
P ₂ O ₅	0.01	0.01	0.01	0.01	0.01	0.01			
Total	95.00	94.86	96.00	95.27	95.52	94.42			
		X-ray	Fluorescence (ppn	a)					
Cr	1.00	6.80	0.00	0.00	1.70	0.00			
Ni	0.00	0.00	0.90	0.00	0.00	0.00			
Cu	59.30	57.80	59.20	56.40	57.50	58.90			
Zn	34.30	25.40	42.10	35.70	24.70	26.70			
Rb	215.40	231.00	214.90	226.80	214.40	206.50			
Sr	27.40	22.40	26.80	25.40	34.40	33.30			
Y	29.10	28.70	34.00	28.20	33.00	38.10			
Zr	85.00	76.70	87.00	78.00	91.90	88.20			
Nb	17.90	17.90	18.30	26.00	29.30	29.70			
La	18.70	20.80	45.70	42.20	12.60	14.00			
Ba	123	171	103	322	78	96			

Appendix 1. Continued.

Tephra-fall sequence (individual pumice fragments)

Sample	P3.3A	P3.3B	P3.4A	P3.4B	P4.1	P4.2D
		Weight 1	Percent Oxide (wt.	%)		
SiO ₂	77.40	77.14	77.15	77.28	77.33	77.25
TiO ₂	0.07	0.07	0.08	0.07	0.07	0.07
Al ₂ O ₃	12.72	12.86	13.04	12.84	12.69	12.69
FeO	0.72	0.83	0.74	0.93	0.76	0.83
MnO	0.06	0.05	0.06	0.06	0.06	0.06
MgO	0.00	0.00	0.03	0.05	0.00	0.00
CaO	0.57	0.59	0.55	0.55	0.58	0.57
Na ₂ O	3.07	2.81	2.58	2.49	2.96	2.93
K ₂ O	5.37	5.63	5.76	5.72	5.53	5.59
P ₂ O ₅	0.01	0.01	0.01	0.01	0.01	0.01
Total	95.37	94.95	94.70	95.67	96.15	95.70
		X-ray	Fluorescence (ppm)			
Cr	9.10	2.20	7.20	0.70	12.00	0.00
Ni	0.00	0.00	0.00	0.00	0.00	0.00
Cu	57.20	56.80	57.20	56.60	56.30	57.80
Zn	21.50	32.70	32.50	31.70	30.80	28.80
Rb	204.00	213.40	220.30	213.10	223.60	224.10
Sr	34.00	35.50	29.00	24.90	24.30	25.70
Y	33.30	35.70	28.10	26.10	26.20	32.20
Zr	77.10	83.10	101.20	99.90	83.30	81.80
Nb	29.40	34.40	24.20	31.90	30.20	34.50
La	9.20	0.20	29.80	30.70	30.10	39.80
Ba	124	59	145	159	157	11

Appendix 1. Continued.

Tephra-fall sequence (individual pumice fragments)

Sample	P4.2G	P4.3A	P4.3C	P5B	P5E	M2G			
Weight Percent Oxide (wt. %)									
SiO ₂	76.86	77.18	77.06	77.29	77.15	76.97			
TiO ₂	0.07	0.07	0.07	0.07	0.07	0.08			
Al ₂ O ₃	13.25	12.75	12.86	12.65	12.76	12.99			
FeO	0.79	0.76	0.81	0.86	0.84	0.79			
MnO	0.06	0.06	0.06	0.06	0.06	0.08			
MgO	0.03	0.00	0.00	0.00	0.05	0.30			
CaO	0.57	0.57	0.58	0.59	0.62	0.50			
Na ₂ O	2.69	3.17	3.02	3.39	3.16	3.18			
K₂O	5.67	5.42	5.53	5.09	5.28	5.10			
P ₂ O ₅	0.01	0.01	0.01	0.01	0.01	0.01			
Total	96.40	96.15	95.63	96.87	96.27	0.00			
		X-ray	Fluorescence (ppm	1)					
Cr	1.70	0.00	0.00	1.50	5.70	0.00			
Ni	0.00	0.00	0.00	0.00	0.00	0.00			
Cu	55.40	55.50	56.90	57.10	57.10	0.00			
Zn	26.30	23.60	41.40	31.00	34.70	56.73			
Rb	237.60	214.70	223.70	206.00	216.70	167.75			
Sr	25.00	24.90	28.80	29.40	36.80	45.24			
Y	28.70	26.10	23.30	26.50	32.60	34.38			
Zr	78.30	78.60	83.50	82.50	81.90	102.22			
Nb	33.00	31.70	30.50	31.00	32.40	19.63			
La	36.00	37.80	19.10	39.40	26.30	80.17			
Ba	136	119	98	105	134	179			

Appendix 1. Continued.

Tephra-fall sequence (individual pumice fragments)

		•	-			
Sample	M4D1	M20B	M21,1C	M21,1D	M21,1E	M21,1H
		Weight	Percent Oxide (wt.	. %)		
SiO ₂	77.15	76.82	76.61	71.12	77.50	75.89
TiO ₂	0.13	0.09	0.12	0.42	0.08	0.12
Al ₂ O ₃	12.75	12.90	13.00	14.78	12.73	13.30
FeO	0.94	0.96	1.10	2.68	0.89	1.18
MnO	0.05	0.09	0.09	0.11	0.08	0.09
MgO	0.04	0.23	0.28	0.64	0.18	0.09
CaO	0.64	0.48	0.63	1.71	0.47	0.64
Na ₂ O	2.32	3.16	3.24	3.87	2.88	3.27
K₂O	5.98	5.25	4.89	4.56	5.17	5.40
P ₂ O ₅	0.00	0.01	0.02	0.11	0.01	0.02
		X-ray	Fluorescence (ppm	1)		
Total	0.00	0.00	0.00	0.00	0.00	0.00
Cr	0.00	0.00	0.00	0.00	0.00	0.00
Ni	0.00	0.00	0.00	0.00	0.00	0.00
Cu	3.21	0.00	0.00	8.16	4.36	0.46
Zn	30.53	57.63	60.12	71.26	54.07	57.61
Rb	141.90	179.81	176.19	130.19	166.42	168.27
Sr	68.64	43.14	78.17	207.55	33.57	101.04
Y	22.04	30.33	28.42	34.85	34.14	35.19
Zr	111.06	107.82	130.05	264.16	96.48	143.01
Nъ	14.27	20.78	22.75	9.12	20.25	18.76
La	71.40	67.77	63.43	104.41	74.61	91.28
Ba	464	269	292	816	160	375

Appendix 1. Continued.

Tephra-fall sequence (individual pumice fragments)

Sample	M21,1I	M21,1J	M21,2I	M21,2H	M4A	M4B			
Weight Percent Oxide (wt. %)									
SiO ₂	69.10	76.95	77.18	76.93	76.29	76.70			
TiO ₂	0.61	0.10	0.08	80.0	0.13	0.13			
Al ₂ O ₃	16.13	12.78	12.95	13.09	13.53	13.07			
FeO	3.27	1.00	0.80	0.81	1.06	0.93			
MnO	0.10	0.08	80.0	0.08	0.05	0.05			
MgO	0.78	0.18	0.43	0.32	0.12	0.08			
CaO	2.32	0.53	0.48	0.53	0.64	0.65			
Na ₂ O	3.66	3.26	2.97	3.08	2.38	2.47			
K₂O	3.86	5.11	5.00	5.07	5.79	5.90			
P ₂ O ₅	0.17	0.01	0.01	0.01	0.01	0.01			
Total	0.00	0.00	0.00	0.00	0.00	0.00			
		Х-г	sy Fluorescence (ppn	n)					
Cr	0.00	0.00	0.00	0.00	0.00	0.00			
Ni	0.00	2.38	0.00	0.00	0.00	0.00			
Cu	4.85	11.69	0.00	0.00	0.00	12.88			
Zn	68.87	56.27	52.97	54.60	88.25	32.80			
Rb	103.38	164.70	164.54	166.76	149.01	154.81			
Sr	334.70	42.13	41.21	46.69	69.90	67.35			
Y	33.05	34.07	33.44	32.66	13.44	18.01			
Zr	316.74	104.94	93.87	102.00	117.89	118.81			
Nb	18.66	19.55	23.79	11.13	13.59	16.70			
La	145.83	86.56	54.95	79.06	104.95	89.35			
Ba	887	319	162	136	555	360			

Appendix 1. Continued.

Tephra-fall sequence (individual pumice fragments)

Sample	M22,1B	M22,1C	M22,1E	M22-3-1	M22-3-2	M22-3-3			
Weight Percent Oxide (wt. %)									
SiO ₂	75.16	74.91	76.04	75.50	75.44	76.36			
TiO ₂	0.11	0.14	0.10	0.11	0.12	0.09			
Al ₂ O ₃	13.87	13.96	13.12	13.25	13.58	13.14			
FeO ·	1.24	1.33	1.05	1.16	1.13	1.05			
MnO	0.08	0.08	80.0	0.08	0.08	0.08			
MgO	0.10	0.06	0.03	0.02	0.13	0.05			
CaO	0.59	0.64	0.51	0.80	0.52	0.49			
Na ₂ O	3.41	3.54	3.62	3.25	3.40	3.41			
K₂O	5.42	5.32	5.43	5.81	5.60	5.32			
P ₂ O ₅	0.01	0.01	0.01	0.01	0.01	0.01			
Total	0.00	0.00	0.00	0.00	0.00	0.00			
		X-ray	Fluorescence (ppm)					
Cr	11.30	7.07	6.32	3.11	0.40	10.87			
Ni	0.00	0.00	0.00	5.08	0.00	1.83			
Cu	0.00	0.00	0.00	6.36	0.00	0.00			
Zn	70.76	61.10	57.39	57.27	62.10	55.84			
Rb	155.04	149.38	158.40	209.70	164.85	154.15			
Sr	40.25	38.77	17.96	160.68	28.05	15.41			
Y	38.91	36.06	39.43	42.71	40.19	38.82			
Zr	184.65	183.28	145.40	169.39	165.52	142.86			
Nb	20.09	21.69	27.00	21.81	26.21	12.63			
La	72.61	61.80	18.71	51.94	64.16	39.43			
Ba	169	191	120	155	0	130			

Appendix 1. Continued.

Tephra-fall sequence (individual pumice fragments)

Sample	M4C-1	M4C-2	M4D-2	M4F	M13A	M20C
		Weight	Percent Oxide (wt.	%)		
SiO ₂	76.59	76.59	75.75	77.21	75.27	76.67
TiO ₂	0.13	0.14	0.16	0.12	0.16	0.08
Al ₂ O ₃	13.17	13.01	13.64	12.79	14.32	12.86
FeO	0.97	1.00	1.27	0.85	1.36	0.82
MnO	0.05	0.05	0.05	0.05	0.07	0.08
MgO	0.09	0.07	0.20	0.05	0.68	0.04
CaO	0.65	0.65	0.67	0.67	0.72	0.51
Na ₂ O	2.46	2.61	2.68	2.49	2.73	3.65
K ₂ O	5.87	5.86	5.57	5.76	4.67	5.27
P ₂ O ₅	0.01	0.01	0.01	0.01	0.01	0.00
Total	0.00	0.00	0.00	0.00	0.00	0.00
		X-ray	Fluorescence (ppn	n)		
Cr	0.00	0.00	0.00	1.25	0.00	0.00
Ni	0.00	0.00	6.66	0.00	0.00	0.00
Cu	8.06	0.00	55.55	0.00	13.29	1.04
Zn	35.35	34.84	40.51	32.68	46.68	49.90
Rb	154.13	155.33	160.57	143.33	158.00	182.16
Sr	68.38	66.11	75.23	68.58	83.38	45.43
Y	20.91	18.12	20.44	23.72	23.06	31.49
Zr	113.58	116.12	130.59	109.00	147.21	114.18
Nb	17.52	14.24	16.54	18.16	10.85	21.25
La	63.93	78.01	76.64	59.45	58.77	60.96
Ba	369	377	352	415	184	155

Appendix 1. Continued.

Tephra-fall sequence (individual pumice fragments)

Sample	M22-3-4	M22-3-5	M22-3-5 M22-3-6		M22-4-1 M22-4-2	
		Weight	Percent Oxide (wt.	%)		
SiO ₂	75.90	76.27	75.84	75.39	75.88	76.13
TiO ₂	0.10	0.10	0.09	0.10	0.09	0.09
Al ₂ O ₃	13.40	13.13	13.42	13.80	13.40	13.49
FeO	1.15	1.08	1.08	1.14	1.07	1.05
MnO	0.08	0.08	0.08	0.08	0.08	0.08
MgO	0.03	0.03	0.07	0.25	0.17	0.23
CaO	0.52	0.49	0.49	0.51	0.51	0.47
Na ₂ O	3.54	3.53	3.53	3.39	3.20	3.26
K ₂ O	5.26	5.28	5.37	5.31	5.57	5.19
P ₂ O ₅	0.01	0.01	0.01	0.01	0.01	0.01
Total	0.00	0.00	0.00	0.00	0.00	0.00
		X-ray	Fluorescence (ppm)		
Cr	3.70	6.10	0.00	4.64	4.15	20.22
Ni	1.27	0.00	1.82	3.59	0.00	0.00
Cu	0.85	0.00	0.00	0.00	3.24	0.00
Zn	57.42	64.04	61.43	62.32	53.94	61.01
Rb	155.69	158.79	158.23	159.17	177.17	155.24
Sr	18.47	14.87	14.81	23.53	19.32	14.80
Y	41.35	42.98	42.20	39.95	37.93	39.06
Zr	158.55	143.06	140.48	164.40	149.10	141.99
Nb	22.16	21.34	23.56	22.71	25.68	24.59
La	42.36	35.41	32.57	49.47	46.91	15.77
Ba	25	116	60	0	0	

ŧ

Tephra-fall sequence (individual pumice fragments)

Sample	mple M22-4-5		M22-4-6 M23-1-1		M25-1-1	M25-1-2	
		Weight	Percent Oxide (wt	. %)			
SiO ₂	75.02	76.22	75.06	74.57	77.12	77.68	
TiO ₂	0.10	0.09	0.09	0.12	0.06	0.07	
Al ₂ O ₃	13.98	13.37	13.67	13.83	12.89	12.48	
FeO	1.22	1.11	1.17	1.32	0.66	0.70	
MnO	0.08	0.08	0.08	80.0	0.07	0.06	
MgO	0.18	0.25	0.05	0.06	0.00	0.00	
CaO	0.55	0.49	0.60	0.67	0.61	0.64	
Na ₂ O	3.49	3.18	3.97	4.05	3.10	2.73	
K ₂ O	5.37	5.19	5.29	5.28	5.47	5.63	
P ₂ O ₃	0.01	0.01	0.01	0.01	0.01	0.01	
Total	0.00	0.00	0.00	0.00	0.00	0.00	
		х	-ray Fluorescence				
Cr	11.91	13.36	18.77	13.95	13.90	7.24	
Ni	0.00	0.00	5.31	0.00	0.00	0.00	
Cu	2.80	17.76	0.00	0.71	2.19	0.00	
Zn	57.51	97.02	66.09	54.93	31.51	31.54	
Rb	153.88	151.93	157.48	151.31	235.08	218.66	
Sr	29.65	17.86	32.29	42.17	24.94	37.11	
Y	39.70	40.44	43.15	40.49	31.72	26.77	
Zr	165.90	146.39	163.44	182.14	64.62	60.28	
Nb	23.54	25.75	22.94	10.34	15.02	16.37	
La	53.23	29.77	17.96	102.73	2.49	35.99	
Ba	256	49	41	48	0	0	

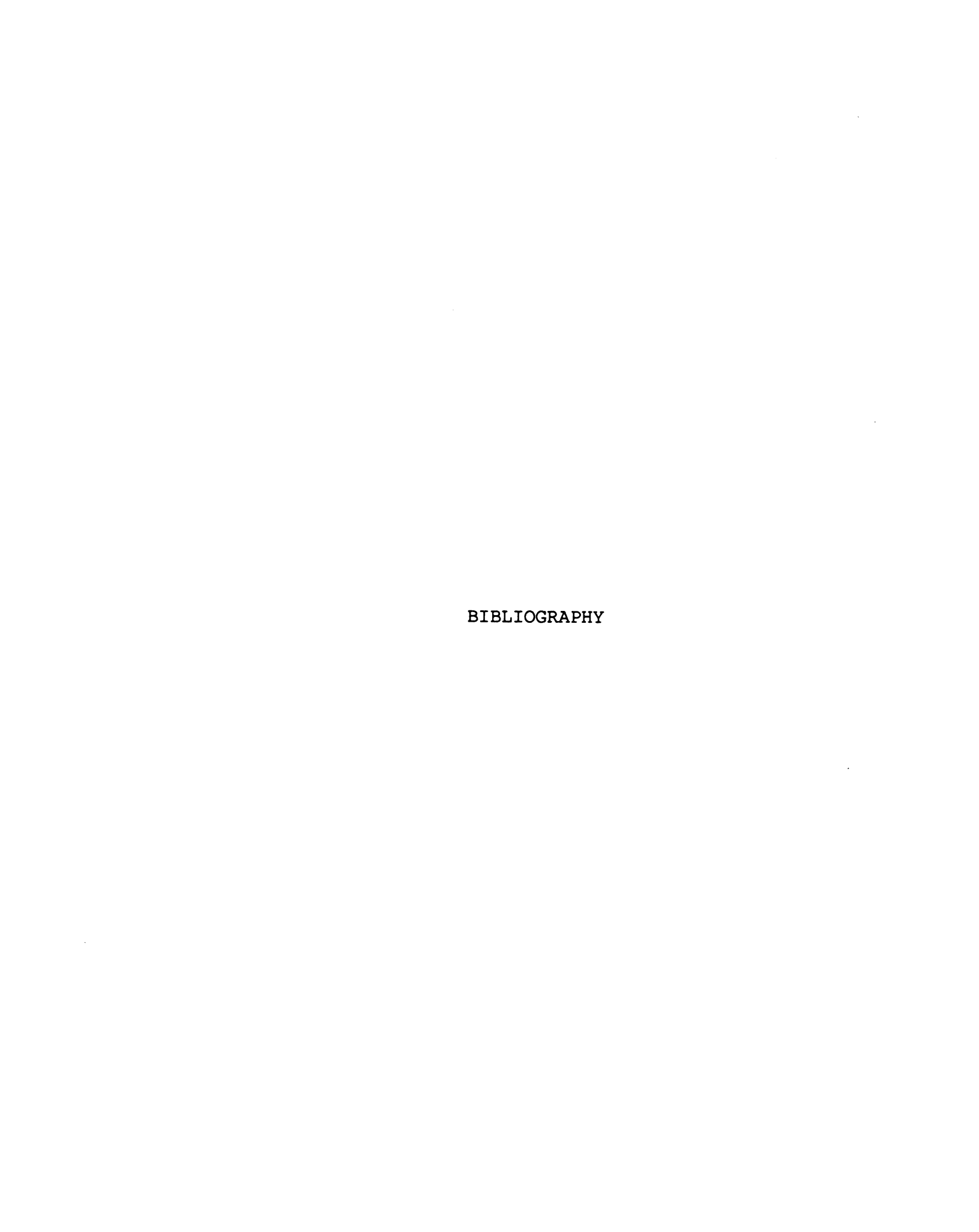
Appendix 1. Continued.

Tephra-fall sequence (individual pumice fragments)

Sample	M25-1-3	
	Weight Percent Oxide (wt. %)	
SiO ₂	77.22	
TiO ₂	0.06	
Al ₂ O ₃	12.71	
FeO	0.71	
MnO	0.06	
MgO	0.00	
CaO	0.63	
Na ₂ O	3.08	
K₂O	5.51	
P _z O ₅	0.01	
Total	0.00	_
	X-ray Fluorescence (ppm)	_
Cr	8.43	_
Ni	0.00	
Cu	2.33	
Zn	27.93	
Rb	230.41	
Sr	37.43	
Y	25.80	
Zr	61.77	
Nb	17.66	
La	28.89	
Ba	62	

Appendix 2. Average error of standard whole rock INAA analyses. Standard concentrations are from Govindaraju, 1989.

Whole Rock Standards used for INAA										
	RGM-1		SY-2		STM-1		₩-2		G-1	
	Conc. (ppm)	Av. error (ppm)	Coac. (ppm)	Av. error (ppm)	Conc. (ppm)	Av. error (ppm)	Conc. (ppm)	Av. error (ppm)	Conc. (ppm)	Av. error (ppm)
Sm	4.30	.60	120.00	3.20	13.00	1.10	3.30	1.40	8.30	1.90
La	23.00	.40	74.00	3.10	150.00	2.40	10.40	1.50	-	
Eu	.70	.02	2.50	.17	3.70	.10	1.10	.04	-	•
Hf	6.00	.20	•	•	27.00	.70	2.60	.20		
Ce	48.00	1.20	•	•	•	•	23.00	1.50	173.00	13.60
Υъ	2.50	.10		•	4.30	.10	2.10	.10	•	•
Lu	•	•	•	•	.66	.08	.33	.01	.16	.01
Th	15.00	2.60	•	•	31.00	4.30	2.40	.50	•	•
Cr	4.00	.90	•	•	4.00	2.50	92.00	8.30	20.00	4.10
Ba	807.00	72.00	•	•	560.00	40.00	182.00	34.70	1080.00	93.00
Cs	9.60	1.00	2.40	.30	1.54	.40	.99	.27	1.60	.10
Sc	4.70	1.10	27.00	1.50	.70	.40	36.00	24.00	2.80	.73
Ta	.97	.07	•	•	•	•	.50	.03	1.50	.15
Ть	-	-	•	-	1.60	.02	.66	.09	.58	.67



BIBLIOGRAPHY

- Blake, S., 1981, Eruptions from zoned magma chambers: Journal of the Geological Society of London, v. 138, p. 281-287.
- Blake, S., and Ivey, N., 1986, Magma-mixing and the dynamics of withdrawal from stratified reservoirs: Journal of Volcanology and Geothermal Research, v. 30, p. 201-230.
- Broxton, D.E., Warren, R.G., Byers, F.M., Jr., and Scott, R.B., 1989, Chemical and mineralogic trends within the Timber Mountain-Oaisis Valley caldera complex, Nevada; evidence for multiple cycles of chemical evolution in a long-lived silicic magma system: Journal of Geophysical Research, v. 94, p. 5943-5960.
- Byers, F.M., Jr., Carr, W.J., and Orkild, P.P., 1989, Volcanic centers of southwestern Nevada: evolution of understanding, 1960-1988: Journal of Geophysical Research, v. 94, p. 5908-5924.
- Cas, R.A.F., and Wright, J.V., 1987, Volcanic Successions: Allen and Unwin, 528 p.
- Civetta, L., Galati, R., and Santacroce, R., 1991, Magma mixing and convictive compositional layering within the Vesuvius magma chamber: Journal of Volcanology, v. 53, p. 287-300.
- Cook, E.F., ed., 1966, Tufflavas and Ignimbrites: Elsevier, 212 p.
- Donnelly-Nolan, J.M., 1988, A magmatic model of Medicine Lake Volcano, California: Journal of Geophysical Research, v. 93, p. 4412-4420.
- Duffield, W.A., and Ruiz, J., 1992, Evidence for the reversal of gradients in the uppermost parts of silicic magma reservoirs: Geology, v. 20, p. 1115-1118.
- Dunbar, N.W., and Hervig, R.L., 1992, Volatile and trace element compositions of melt inclusions from the Lower Bandelier Tuff: Implications for magma chamber processes and eruptive style: Journal of Geophysical Research, v.97, p. 15,151-15,170.

- Farmer, G.L., Broxton, D.E., Warren, R.G., and Pickthorn, W., 1991, Nd, Sr, and O isotopic variations in metaluminous ash-flow tuffs and related volcanic rocks at the Timber Mountain/Oasis Valley Caldera, Complex, SW Nevada: implications for the origin and evolution of large-volume silicic magma bodies: Contributions to Mineralogy and Petrology, v. 109, p. 53-68.
- Feeley, T.C., and Grunder, A.L., 1991, Mantle contribution to the evolution of Middle Tertiary silicic magmatism during early stages of extension: the Egan Range volcanic complex,, east-central Nevada: Contributions to Mineralogy and Petrology, v. 106, p. 154-169.
- Fisher, R.V., and Schmincke, H.U., 1984, Pyroclastic Rocks: Springer-Verlag, 472 p.
- Flood, T.P., 1987, Cyclic evolution of a magmatic system: The Paintbrush Tuff, SW Nevada Volcanic Field [Ph.D. Thesis]: East Lansing, Michigan, Michigan State University, 147 p.
- Flood, T.P., Schuraytz, B.C., Vogel, T.A., 1989, Magma mixing due to disruption of a layered magma body: Journal of Volcanology and Geothermal Research, v. 36, p. 241-255.
- Flood, T.P., Vogel, T.A., and Schuraytz, B.C., 1989, Chemical evolution of a magmatic system: The Paintbrush Tuff, Southwest Nevada Volcanic Field: Journal of Geophysical Research, v. 94, p. 5943-5960.
- Gardner, J.E., Sigurdsson, H., and Carey, S.N., 1991, Eruption dynamics and magma withdrawal during the plinian phase of the Bishop Tuff Eruption, Lang Valley Caldera: Journal of Geophysical Research, v. 96, p. 8097-8111.
- Govindaraju, K., ed., Geostandards Newsletter, Special Issue v. 13, 1989.
- Grunder, A.G., and Mahood, G.A., 1988, Physical and chemical models of zoned silicic magmas: the Loma Seca Tuff and Calabozos Caldera, Southern Andes: Journal of Petrology, v. 29, no. 4, p. 831-867.
- Hahn, G.A., Rose, W.I., Jr., and Meyers, T., 1979, Geochemical correlation of genetically related rhyolitic ash-flow and air-fall ashes, central and western Guatemala and the equatorial Pacific: Geological Society of America Special Paper 180, p. 101-112.

- Hervig, R.L., and Dunbar, N.W., 1992, Cause of chemical zoning in the Bishop (California) and Bandelier (New Mexico) magma chambers, Earth and Planetary Science Letters, v. 111, p. 97-108.
- Hildreth, E.W., 1979, The Bishop Tuff: Evidence for the origin of compositional zonation in silicic magma chambers: Geological Society of America Special Paper 180, p. 43-75.
- Hildreth, W., 1981, Gradients in silicic magma chambers: implications for lithospheric magmatism: Journal of Geophysical Research, v. 86, p. 10153-10192.
- Hildreth, W., Halliday, A.N., and Christiansen, R.L., 1991, Isotopic and chemical evidence concerning the genesis and contamination of basaltic and rhyolitic magma beneath the Yellowstone Plateau Volcanic Field: Journal of Petrology, v. 32, part 1, p. 63-138.
- Huijsmans, J.P., and Barton, M. 1989, Polybaric geochemical evolution of two shield volcanoes from Santorini, Aegean Sea, Greece; evidence for zoned magma chambers from cyclic compositional variations: Journal of Petrology, v. 30, no. 3, p. 583-625.
- Huysken, K.T., and Vogel, T.A., 1992, Pre-caldera forming pyroclastic deposits: Implications for the origin of the large volume Rainier Mesa ash-flow sheet: Geological Society of America, Abstracts with Programs, v. 24, p. 176.
- Huysken, K.T., and Vogel, T.A., 1991, Early eruptions from the Rainier Mesa Magma Body: Implications for complex withdrawal from a layered system: American Geophysical Union, Transactions (EOS), v. 72, p. 576.
- Lu, F., 1991, The Bishop Tuff: Origins of the high-silica rhyolite and its thermal and compositional zonations: Ph.D. Thesis, Chicago Illinios, The University of Chicago, 331 p.
- Mills, J.G., Jr., 1991, The Timber Mountain Tuff, southwestern Nevada Volcanic Field: Geochemistry, mineralogy and petrogenesis [Ph.D. Thesis]: East Lansing, Michigan, Michigan State University, 332 p.
- Mills, J.G., Jr., and Vogel, T.A., 1988, Compositional interfaces in magma bodies: geothermometers of Fe-Ti oxides in glassy pumice fragments: American Geophysical Union, Trans (EOS), v. 69, p. 526.

- Mills, J.G., Jr., Schuraytz, B.C., Flood, T.P., Rose, T.P., and Vogel, T.A., 1987, Evolution of a zoned magmatic system in the Southwestern Nevada Volcanic Field: Geological Society of America, Abstracts with Programs, v. 19, p. 773.
- Qin, Z., Lu, F., and Anderson, A.T., Jr., 1992, Diffusive reequilibration of melt and fluid inclusions: American Mineralogist, v. 77, p. 565-576.
- Rose, T.P., 1988, A model for the origin of the chemically zoned Ammonia Tanks Member of the Timber Mountain Tuff due to crystal fractionation [Master's Thesis]: East Lansing, Michigan, Michigan State University, 72 p.
- Sawyer, D.A., and Sargent, K.A., 1989, Petrologic evolution of divergent peralkaline magmas from the Silent Canyon Caldera Complex, Southwestern Nevada Volcanic Field: Journal of Geophysical Research, v. 94, p. 6021-6040.
- Schuraytz, B.C., 1988, Geochemical gradients in the Topopah Spring Member of the Paintbrush Tuff: Evidence for eruption across a magmatic interface [Ph.D. Thesis]: East Lansing, Michigan, Michigan State University, 148 p.
- Schuraytz, B.C., Vogel, T.A., and Younker, L.W., 1989, Evidence for dynamic withdrawal from a layered magma body: The Topopah Spring Tuff, southwestern Nevada: Journal of Geophysical Research, v. 94, p. 5925-5942.
- Scott, R.B., Byers, F.M., Jr., and Warren, R.G., 1984, Evolution of magma below clustered calderas, Southwest Nevada Volcanic Field: Eos, Transactions, American Geophysical Union, v. 65, no. 45, p. 1126-1127.
- Smith, R.L., 1979, Ash-flow magmatism: Geological Society of America Special Paper 180, p. 5-27.
- Spera, F.J., Oldenburg, C.M., and Yuen, D.A., 1989, Magma zonation; effects of chemical buoyancy and diffusion: Geophysical Research Letters, v. 16, no. 12, p. 1387-1390.
- Spera, F.J., Yuen, D.A., Greer, J.C., and, Sewell, G., 1986, Dynamics of magma withdrawal from stratified magma chambers, Geology, v. 14, p. 723-726.

- Stix, J., Goff, F., Gorton, M.P, Heiken, G., and Garcia, S.R., 1988, Restoration of compositional zonation in the Bandelier silicic magma chamber between two caldera-forming eruptions: Geochemistry and origin of the Cerro Toledo Rhyolite, Jamez Mountains, New Mexico, U.S.A.: Journal of Geophysical Research, v. 93, p. 6129-6147.
- Stix, J., and Gorton, M.P., 1990, Changes in silicic melt structure between the two Bandelier caldera-forming eruptions, New Mexico, USA: Evidence from Zirconium and light rare earth elements: Journal of Petrology, v. 31, p. 1261-1283.
- Trial, A.F., and Spera, F.J., 1990, Mechanisms for the generation of compositional heterogeneities in magma chambers: Geological Society of America Bulletin, v. 102, p. 353-367.
- Valentine, G.A., Wohletz, K.H., 1991, Sources of unsteady column dynamics in pyroclastic flow eruptions: Journal of Geophysical Research, v. 96, p.21,887-21,892.
- Valentine, G.A., Wohletz, K.H., and Kieffer, S.W., 1992, Effects of topography on facies and compositional zonation in caldera-related ignimbrites: Geological Society of America Bulletin, v. 104, p.154-165.
- Vogel, T.A., Ryerson, F.J., Noble, D.C., and Younker, L.W., 1987, Limits to Magma Mixing Based on Chemistry and Mineralogy of Pumice Fragments: Journal of Geology, v. 95, p. 659-670.
- Vogel, T.A., Eichelberger, J.C., Younker, L.W., Schuraytz, B.C., Horkowitz, J.P., Stockman, H.W., and Westrich, H.R., 1989, Petrology and Emplacement Dynamics of the Intrusive and Extrusive Rhyolites of Obsisian Dome Inyo Craters Volcanic Chain, Eastern California: Journal of Geophysical Research, v. 94, p. 6041-6058.
- Vogel, T.A., Noble, D.C., and Younker, L.W., 1989, Evolution of a chemically zoned magma body: Black Mountain Volcanic Center, southwestern Nevada: Journal of Geophysical Research, v. 94, no. B5, p. 6041-6058.
- Vogel, T.A., Ryerson, F.J., Noble, D.C., and Younker, L.W., 1987, Limits to magma mixing based on chemistry and mineralogy of pumice fragments erupted from a chemically zoned magma body: Journal of Geology, v. 95, p.659-670.

- Warren, R.G., Byers, F.M., Jr., Broxton, D.E., Freeman, S.H. and Hagan, R.C., 1989, Phenocryst abundances and glass and phenocryst compositions as indicators of magmatic environments of large-volume ash-flow sheets in southwestern Nevada: Journal of Geophysical Research, v 94, no. B5, p. 5987-6020.
- Warren, R.G., and Valentine, G.A., 1990, Precursor eruptive activity of the large-volume Rainier Mesa Tuff, southwestern Nevada, U.S.A., [abstract]: New Mexico Bureau of Mines and Meneral Resources Bulletin 131, p. 287.
- Weiss S.I., and Noble, D.C., 1989, Stonewall Mountain Volcanic Center, southern Nevada: stratigraphic, structural, and facies relations of outflow sheets, near-vent tuffs, and intracaldera units: Journal of Geophysical Research, v. 94, no. B5, p. 6059-6074.
- Weiss, S.I., Noble, D.C., and McKee, E.H., 1989, Paleomagnetic and cooling constraints on the duration of the Pahute Mesa-Trail Ridge eruptive event and associated magmatic evolution, Black Mountain Volcanic Center, southwestern Nevada: Journal of Geophysical Research, v. 94, no. B5, p.6075-6084.
- Whitney, J.A., Dorais, M.J., Stormer, J.C., Jr., Kline, S.W., and Matty, D.J., 1988, Magmatic conditions and development of chemical zonation in the Carpenter Ridge Tuff, Central San Juan Volcanic Field, Colorado: American Journal of Science, v. 288a, p. 16-44.
- Widom, E., Schmincke, H.-U., and Gill, J.B., 1992, Processes and timescales in the evolution of a chemically zoned trachyte: Fogo A, Sao Miguel, Azores: Contributions to Mineralogy and Petrology, v. 111, p. 311-328.
- Worner G., and Schmincke, H.-U., 1984, Mineralogical and Chemical Zonation of the Laacher See Tephra Sequence (East Eifel, W. Germany): Journal of Petrology, v. 25, p. 805-835.

MICHIGAN STATE UNIV. LIBRARIES
31293008913588